A Laterally Interconnected Neural Architecture in MST Accounts for Psychophysical Discrimination of Complex Motion Patterns

SCOTT A. BEARDSLEY AND LUCIA M. VAINA
Brain and Vision Research Laboratory, Department of Biomedical Engineering,
Boston University, Boston, MA 02215
vaina@bu.edu

Action Editor: Jonathan Victor

Abstract. The complex patterns of visual motion formed across the retina during self-motion, often referred to as *optic flow*, provide a rich source of information describing our dynamic relationship within the environment. Psychophysical studies indicate the existence of specialized detectors for component motion patterns (radial, circular, planar) that are consistent with the visual motion properties of cells in the medial superior temporal area (MST) of nonhuman primates. Here we use computational modeling and psychophysics to investigate the structural and functional role of these specialized detectors in performing a graded motion pattern (GMP) discrimination task. In the psychophysical task perceptual discrimination varied significantly with the type of motion pattern presented, suggesting perceptual correlates to the preferred motion bias reported in MST. Simulated perceptual discrimination in a population of independent MST-like neural responses showed inconsistent psychophysical performance that varied as a function of the visual motion properties within the population code. Robust psychophysical performance was achieved by fully interconnecting neural populations such that they inhibited nonpreferred units. Taken together, these results suggest that robust processing of the complex motion patterns associated with self-motion and optic flow may be mediated by an inhibitory structure of neural interactions in MST.

1. Introduction

The motion of the visual scene across the retina, termed *optic flow*, contains a wealth of information describing our dynamic relationship within the environment. Perceptual information regarding heading, time to contact, object motion, and object segmentation can all be recovered to various degrees by analyzing the complex motion components comprising optic flow (for a review, see Andersen, 1997; Lappe et al., 1999). While the usefulness of such information is clear, the mechanisms underlying its processing and extraction are still poorly understood. Recent psychophysical and neurophysiological studies have begun to address these

issues by defining how optic flow is processed and where such processing may occur (Andersen et al., 2000; Bremmer et al., 2000; Duffy, 2000; Lappe, 2000; van den Berg, 2000; for a review see Vaina, 1998).

Psychophysical studies indicate the existence of specialized detectors in the human visual system that are selective for the radial, circular, and planar motion components associated with optic flow (Freeman and Harris, 1992; Regan and Beverley, 1979; Snowden and Milne, 1996; Te Pas et al., 1996). Perceptually, these motion-pattern mechanisms have been shown to integrate local motions along complex trajectories to obtain global motion percepts over wide visual fields (Burr et al., 1998; Morrone et al., 1995).

Early studies by Regan and Beverley (Regan and Beverley, 1978, 1979, 1985) showed that adaptation to expanding (looming) and contracting stimuli decreased sensitivity to motion patterns in a manner that was inconsistent with local motion mechanisms. Furthermore, they showed that adaptation to expanding stimuli does not affect sensitivity to contracting or rotating stimuli, suggesting a set of global motion mechanisms, distinct from local mechanisms encoding direction and speed, that process visual motion patterns independent of one another. Snowden and Milne (1996) later examined motion-pattern detection thresholds with and without prior motion adaptation and showed that detection thresholds for unadapted motion patterns were independent of the adapted motion provided the motion patterns were dissimilar. As the similarity between adapted and unadapted motion patterns increased, unadapted detection thresholds smoothly increased to levels consistent with the adapted motion. These results suggest the existence of a more extended set of motion-pattern mechanisms that include specialized detectors for spiral motions.

Single-cell studies in nonhuman primates have identified possible neural correlates to these perceptual mechanisms in visual motion areas that contain neurons responsive to simple motion-pattern components of optic flow. Neurons in the dorsal division of medial superior temporal cortex (MSTd) have large receptive fields and exhibit a continuum of preferred responses to planar, radial, circular, and spiral motion patterns (Duffy and Wurtz, 1991a, 1991b, 1995, 1997; Geesaman and Andersen, 1996; Graziano et al., 1994; Lagae et al., 1994; Orban et al., 1992; Saito et al., 1986; Tanaka et al., 1989; Tanaka and Saito, 1989).

In MSTd, the distribution of preferred motion patterns spans a continuum in the stimulus space formed by radial, circular, and spiral motions that is biased in favor of expanding motions (Geesaman and Andersen, 1996; Graziano et al., 1994). Many cells also respond to planar motion patterns, suggesting a more extensive set of preferred motion classifications within MST that includes the four planar directions of motion (up/down, left/right) (Duffy and Wurtz, 1991a, 1991b, 1997). Within this multidimensional plano-radial-circular space, cells respond across a wide range of stimulus speeds and exhibit speed tuning profiles best characterized by their filtering properties (that is, low-pass, linear, high-pass) (Duffy and Wurtz, 1997; Orban et al., 1995). The preferred pattern responses of these neurons are scale and position invariant to small

and moderate variations in the stimulus size, center-of-motion (COM) location, and visual cues conveying the motion (Geesaman and Andersen, 1996; Graziano et al., 1994; Tanaka and Saito, 1989). For larger variations and with tests using nonoptimal stimuli, cell responses degrade continuously (Duffy and Wurtz, 1995; Graziano et al., 1994). This sensitivity to the global speed and motion-pattern information contained within optic flow has led to speculation that cells in MSTd could be used to encode flow based heading through the visual scene.

Recent computational models of visual motion perception and navigation have begun to provide insight into how perceptually relevant motion information can be encoded in biologically plausible neural structures consistent with visual motion areas such as MST. Early feed-forward models of visual processing from the middle temporal area (MT) to MST have examined the emergence of motion-pattern properties based on the computational pooling of simple direction selective units. Zhang et al. (1993) constructed a Hebbian network that developed position-invariant units exhibiting preferred responses to a continuum of complex motion patterns. However, unlike cells in MSTd, their network decomposed the velocity field, responding to the preferred motion-pattern components regardless of the magnitudes of additional motion-pattern components in the stimulus.

Models using units with more extensive motion-pattern properties have been developed to further refine the nature of the feed-forward mechanisms that contribute to the development of global motion properties (Beardsley and Vaina, 1998; Wang, 1995, 1996). In a supervised network we (Beardsley and Vaina, 1998) identified a majority of hidden units whose position invariance and preferred motion properties were consistent with cells in MSTd, independent of the biases associated with the specification of motion-pattern properties in the output layer. In subsequent simulations, we extended a series of trained networks to simulate psychophysical performance in a motion-pattern discrimination task. Under simulated psychophysical conditions, we demonstrated that the motion-pattern information encoded within small populations of MST-like units was sufficient to obtain perceptual estimates consistent with human performance (Beardsley and Vaina, 1998). Zemel and Sejnowski (1998) identified similar motion-pattern properties in an unsupervised network trained with optic-flow patterns generated from motion through a simulated

environment. For network units containing spatially separated receptive fields, they identified position-invariance properties similar to those in MST and investigated their ability to segment individual motion patterns from a complex motion scene.

Still other biologically inspired models have examined the role of motion-pattern mechanisms in heading estimation (Grossberg et al., 1999; Hatsopoulos and Warren, 1991; Lappe et al., 1996; Perrone and Stone, 1994, 1998), with an emphasis toward understanding the computational mechanisms sufficient to extract perceptually meaningful heading information from optic flow. Using a winner-take-all template model of self-motion estimation, Perrone and Stone (1994, 1998) obtained heading estimates under gaze-stabilization conditions that were well matched to equivalent measures of human performance. Within the template layer they observed motion-pattern properties that were consistent with to cells in MST across a wide range of conditions; suggesting that MST is computationally sufficient to extract accurate heading estimates. While such models typically parallel the biological properties reported in the V1-MT-MST motion processing stream, other less biologically inspired heading networks have also been shown to develop visual motion properties consistent with these cortical areas (Cameron et al., 1998).

Throughout these models, neural structures that parallel the function of the visual motion pathway have been implemented to (1) examine how physiologically observed visual motion properties develop and (2) quantify the computational mechanisms required to extract perceptually useful information from the motion patterns within optic flow. In doing so, they have improved our understanding of visual motion processing; however, they have typically not addressed the computational role of lateral connections *within* the visual motion areas, such as MST and ventral interparietal cortex (VIP), typically associated with flow-specific heading and navigation tasks.

Single-cell studies in nonhuman visual cortex have identified a variety of intrinsic neural structures within early visual motion areas such as the primary visual cortex (V1) and MT (Gilbert et al., 1996; Gilbert, 1992; Kisvarday et al., 1997; Lund et al., 1993; Malach et al., 1997). Extensive modeling of the local lateral connections inherent in these structures, both in V1 (Ben-Yishai et al., 1995; Stemmler et al., 1995; Worgotter et al., 1991) and MT (Koechlin et al., 1999; Liu and Hulle, 1998), suggest the existence of complex

interconnected architectures whose most basic connection profiles can impart considerable computational power to simulated populations of neurons. Combined psychophysical and computational modeling studies support these findings and further suggest that lateral connections may play a significant role in encoding the visual motion properties associated with various psychophysical tasks (Adini et al., 1997; Chey et al., 1998; Koechlin et al., 1999; Nowlan and Sejnowski, 1995; Stemmler et al., 1995).

As the importance of such local interactions has become more clear, attention has begun to focus on their likely structure and function in higher visual motion areas as well (Amir et al., 1993; Edelman, 1996; Miikkulainen and Sirosh, 1996; Sakai and Miyashita, 1991; Taylor and Alavi, 1996; Wiskott and von der Malsburg, 1996). In the model proposed here we examine the influence of simple lateral connection profiles in encoding motion-pattern information within a simulated population of MST neurons.

In the cortex, the interpretation of psychophysical and physiological data within a neural framework depends on how the information is represented (for a review see deCharms and Zador, 2000). Although precise temporal codes are capable of transmitting large amounts of information between individual neurons, there is good evidence that cortical neurons represent information using a coarse population code of redundant units (Shadlen and Newsome, 1994, 1998; Softky, 1995; Softky and Koch, 1993).

Indirect support for information transfer via populations of noisy cortical units has come from studies demonstrating how perceptually useful information can be extracted from the underlying neural representation (Seung and Sompolinsky, 1993; Snippe, 1996). The use of population coding techniques to decode perceptually relevant information has been proposed across a wide range of processing modalities including motor planning for reaching (Georgopoulos et al., 1986, 1988, Lukashin and Georgopoulos, 1993, 1994; Lukashin et al., 1996; Salinas and Abbott, 1994, 1995), visual orientation discrimination, and visual motion-direction discrimination (Sundareswaran and Vaina, 1995, 1996; Vaina et al., 1995; Zemel et al., 1998; Zohary, 1992).

While there is widespread support for population codes in biological systems, optimal methods for decoding the neural information remain unclear. A variety of decoding techniques have been proposed including Bayesian inference (Foldiak, 1993; Oram et al., 1998),

population vector analysis (Seung and Sompolinsky, 1993), maximum likelihood (Pouget et al., 1998), center of mass (Snippe, 1996), and probability density estimation (Sanger, 1996; Zemel et al., 1998). However, the computational efficiency and biological plausibility of these methods are often at odds with one another, preventing general acceptance for any one technique.

Here we investigate the computational and functional role of lateral connections *within* a population of MST-like units using population vector analysis to model psychophysical performance during a graded motion pattern (GMP) discrimination task. Specifically, we use discrimination thresholds obtained across eight test motion patterns together with the visual motion properties reported in MST, and refined in a previous model (Beardsley and Vaina, 1998), to quantify the neural connections sufficient to encode perceptual motion information across a population of visually responsive neurons. Discrimination thresholds are then examined as a function of the reported human performance for neural models simulating (1) convergent stimulus information in a population code of independent neural responses, (2) a laterally connected population code incorporating excitatory and inhibitory connections between units, (3) a population of independent thresholded neural responses, and (4) a laterally connected population code incorporating inhibitory connections between units. For each of the above conditions, discrimination thresholds are optimized to the fitted psychophysical performance through the variation of structural parameters used to define the connectivity between units and the influence of each unit on the perceptual estimate. Analysis of the distribution of optimal structural parameters is then used to quantify the neural structures in MST that are sufficient to encode the visual motion information associated with the perceptual task.

A preliminary version of this work was presented at the Association for Research in Vision and Ophthalmology 1999 Annual Meeting (Beardsley et al., 1999).

2. Psychophysics

2.1. Methods

In a temporal two-alternative-forced-choice (2TAFC) graded motion-pattern (GMP) task, we measured discrimination thresholds to global changes in the patterns of complex motion (Beardsley and Vaina, 2001).
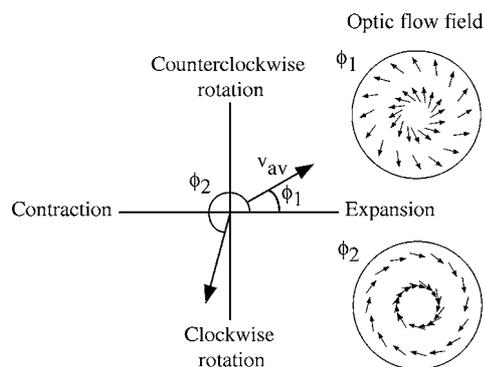
Figure 1. The motion pattern space. Radial, circular, and spiral complex motion patterns are represented as vectors in a 2D stimulus space. The vector magnitude (v_{av}) corresponds to the average dot speed across the motion field, and the flow angle (ϕ) defines the type of motion pattern relative to a 0 deg baseline expansion. Off-axis regions correspond to intermediate degrees of spiral motion.

Stimuli consisted of dynamic random dot displays presented in a 24 deg. annular region, with the central 4 deg. removed, in which each dot moved coherently from frame-to-frame according to the motion equations:

$$\begin{pmatrix} x_{n+1} \\ y_{n+1} \end{pmatrix} = e^{\omega \cos \phi} \begin{pmatrix} x_n \cos(\omega \sin \phi) - y_n \sin(\omega \sin \phi) \\ x_n \sin(\omega \sin \phi) + y_n \cos(\omega \sin \phi) \end{pmatrix}.$$

Within this representation, coherent motion patterns could be uniquely described by their flow angle (ϕ) in the two dimensional (2D) stimulus space formed by cardinal (radial and circular) and spiral motion patterns (Fig. 1). Throughout the task the center of the motion pattern remained centered in the visual display.

Prior to the start of each experiment, observers adapted for 10 sec to the background display in a darkened room. During testing, observers were required to fixate a small central square and pairs of motion patterns were presented using a 2TAFC constant stimulus paradigm (500 msec interpair and interstimulus intervals) with an auditory cue preceding each stimulus. To minimize the buildup of adaptation to specific motion patterns (expansion, clockwise rotation, and so on), opposing motions (such as expansion/contraction) were interleaved across paired presentations.

Discrimination pairs of stimuli were formed by symmetrically perturbing the flow angle of eight test motion patterns (expansion, contraction, clockwise (CW), and counterclockwise (CCW) rotation and the four intermediate spiral motions) by $\pm \phi_p$ in the 2D stimulus
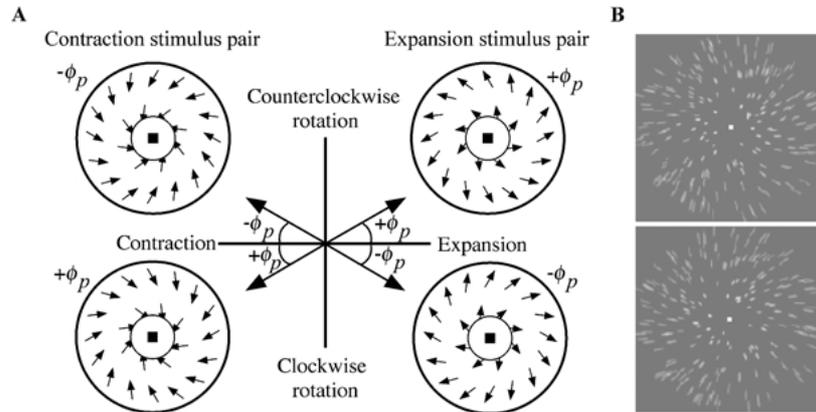
Figure 2. Schematic representation of the graded motion-pattern (GMP) discrimination task for radial motions. Stimuli consisted of random dot kinematograms (RDK) presented on an AppleVision 1710 monitor in a 24 deg diameter annular region (central 4 deg removed) at a 54 cm viewing distance. All stimulus apertures were *illusory* as defined by an absence of dots. RDK movie sequences were generated offline and presented with a screen resolution and refresh rate of 832×624 pixels and 75 Hz, respectively. Each RDK contained a uniform distribution of 190 (9.3 Cd/m^2) motion dots displayed on a low luminance (5.2 Cd/m^2) gray background. At the subject viewing distance each dot subtended $\sim$10 minutes of visual angle and moved through a radial speed gradient whose maximum speed could be varied from 6 to 34.4 deg/sec between tests in a direction consistent with the motion pattern being displayed. Eleven frame dot lifetimes were imposed to reduce local trajectory tracking, and coherent flicker was minimized by uniformly distributing the initial dot lifetimes among the first 11 frames. The experimental task controlled for timing-based discrimination cues by including stimulus duration uncertainties that were proportional to and centered around the nominal stimulus duration (440 ± 40 msec). **A:** Discrimination pairs of stimuli were created by perturbing the flow angle (ϕ) of each test motion by $\pm \phi_p$ in the stimulus space. For the radial test motions shown here, the perturbations are equivalent to the combination of a circular motion component (magnitude $= v_{av}\sin(\phi_p)$) from the nearest circular motion axis with the test motion (magnitude $= v_{av}\cos(\phi_p)$). **B:** A scaled time-lapsed version of a radial stimulus pair.

space. In each paired presentation observers were required to select the stimulus, via key press, containing a negative perturbation relative to the test motion (Fig. 2).

For each observer, the task of discriminating negative/positive perturbations across test motion patterns was facilitated through the presentation of radial, circular, and spiral test motion patterns in separately interleaved blocks of trials. Within each block of trials observers were required to discriminate motion-pattern perturbations using the following conceptual simplifications to the negative perturbation judgment; for radial test motions select the stimulus containing a CCW motion component; for circular test motions select the stimulus containing and expanding motion component; for CCW/expanding and CW/contracting spiral test motions select the stimulus containing the larger radial (expansion or contraction) motion component; for CW/expanding and CCW/contracting spiral motions select the stimulus containing a larger circular (CW or CCW) motion component.
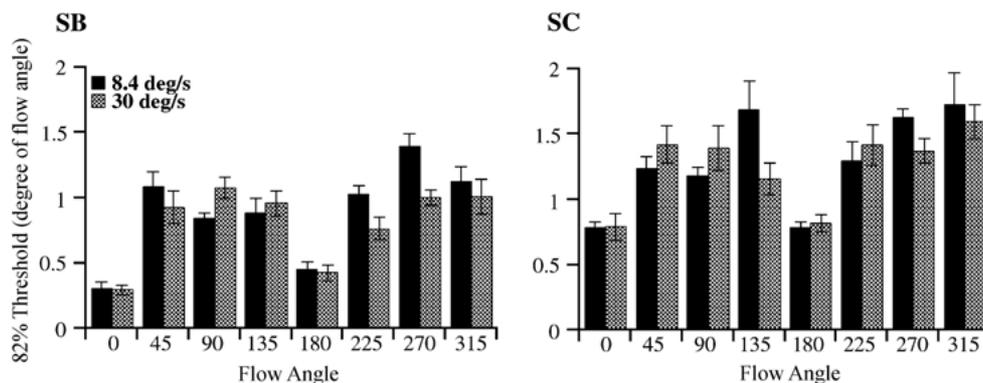
For each observer, discrimination thresholds were obtained at two average dot speeds (8.4 and 30 deg/sec) for each of the eight test motions. Discrimination thresholds were estimated for each constant stimulus

session using a weighted two-parameter Weibull fit to a minimum of four perturbation levels. A χ^2 goodness-of-fit measure was used to exclude data sets with poor curve fits from further analysis.

2.2. Results

Discrimination thresholds across the eight test motion patterns (expansion, contraction CW/CCW rotation, and the four intermediate spiral motions) are reported here on a subset of the observer population (Beardsley and Vaina, 2001) consisting of two experienced psychophysical observers, one of whom was naïve to the purpose of the psychophysical task. For each test condition threshold performance is reported as the mean and standard error averaged across eight to twelve threshold estimates whose χ^2 measures fell below the rejection level ($\chi^2 < \chi_R^2$; $p < 0.1$).

Across observers and mean dot speeds perceptual performance followed a distinct trend in the stimulus space with discrimination thresholds for radial motion patterns (expansion/contraction) significantly lower than thresholds for circular motion patterns (CW/CCW rotation) ($p < 0.001$; $t(3.39)$ d.f. $= 37$)

Figure 3. GMP discrimination thresholds. Thresholds and standard errors across eight test motions (radial, circular, and the four intermediate spiral motions) at two mean dot speeds (8.4 and 30 deg/s) for two observers (SB and SC). Performance varied continuously as a function of the test motion pattern for both dot speeds with radial motion thresholds ($\phi = 0, 180$) significantly lower than circular motion thresholds ($\phi = 90, 270$) ($p < 0.001$; $t(3.3908)$ d.f. $= 37$). Thresholds for the intermediate spiral motions were not significantly different from circular motion patterns ($p = 0.223$, $t(0.7458)$ d.f. $= 60$); however, the trends across test motions were well fit (SB: $r > 0.82$, SC: $r > 0.77$) by sinusoids whose period and phase were approximately 196 ± 10 deg and -72 ± 20 deg, respectively.

(Fig. 3). Within these subpairs, thresholds for radial and circular motion patterns were well matched ($\phi_p \sim 0.25$ to 0.5 deg and $\phi_p \sim 1$ to 1.5 deg, respectively) across observers. Figure 3 also shows that while the individual thresholds for the intermediate spiral motions were not significantly different from circular motion patterns ($p = 0.223$, $t(0.7458)$ d.f. $= 60$), the trends across test motions were well fit (SB: $r > 0.82$, SC: $r > 0.77$ by sinusoids whose period and phase were approximately 198 ± 20 deg and -75 ± 41 deg respectively.

Comparable trends in performance were also obtained for stimuli containing 50% flicker noise (data not shown). In this condition, dot motions were randomly assigned as signal or noise from frame-to-frame such that the proportion of signal dots in each frame was 50%. Across the population of dots, this resulted in a decreasing probability of uninterrupted local motion that was structurally similar to the two-frame dot motion stimuli used previously to quantify the existence of specialized motion-pattern mechanisms (Burr et al., 1998; Morrone et al., 1995).

The consistency of the sinusoidal trend across observers suggests a continuum of perceptual performance in which GMP discrimination is poorest for circular motions and best for radial motions. The continued presence of statistically significant differences across motion patterns, both in the presence of the 360° range of local motion trajectories in each stimulus and the subsequent reduction of local motion signal for the 50% flicker noise condition, argue against a primary role for local motion mechanisms in the perceptual task. These results, together with similar perceptual studies reporting the existence of a more global set of motion pattern mechanisms (Burr et al., 1998; Morrone et al., 1995; Regan and Beverley, 1979; Snowden and Milne, 1996), suggest that the threshold differences may be associated with variations in the motion properties across a series of global mechanisms tuned to different motion-pattern components.

3. Computational Modeling

3.1. Methods

3.1.1. Discriminating Motion Patterns via a Population Code of Neural Responses. The similarities between the visual motion patterns used to quantify human perception and the tuning properties of cells in MST and VIP suggest that these cortical regions may mediate the perceptual task. If, for example, motion-pattern perception were based on a simple population code of complex motion detectors drawn from the anisotropic cell distribution reported in MST (Geesaman and Andersen, 1996; Graziano et al., 1994), one might expect that motion-pattern discriminability should follow a distribution symmetric about the radial motion axis (in the 2D motion pattern space) with expansion thresholds lowest and contraction thresholds among the highest. Within this framework, variations in human performance mediated by a simple population code of independent neural responses would require the presence of neural interactions within the
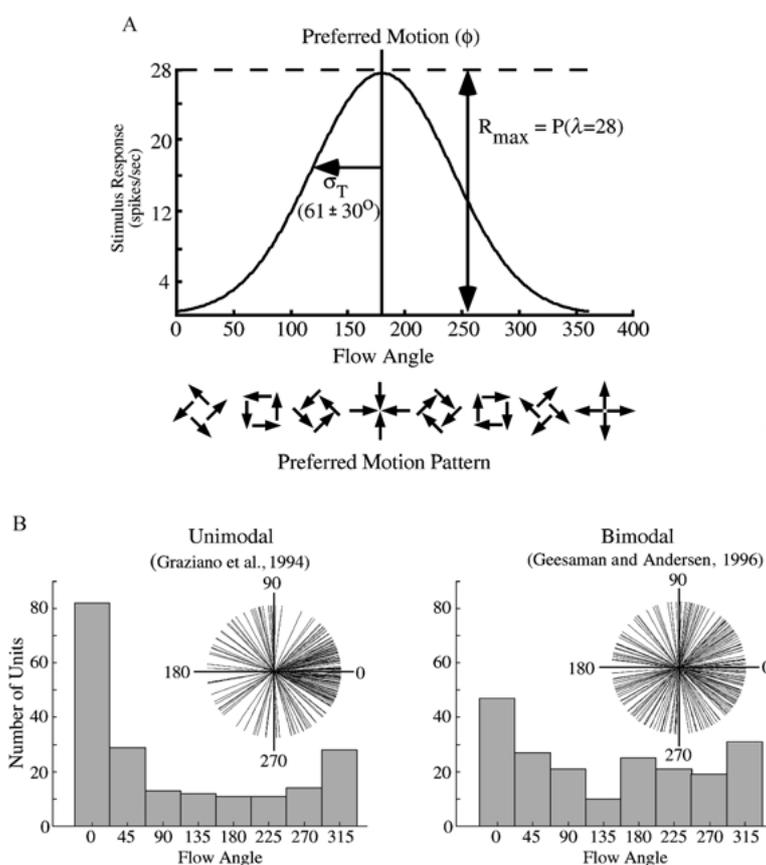
Figure 4.   Motion pattern properties of the MST-like units used to model the psychophysical task. **A:** Motion-pattern tuning followed a gaussian profile ($\sigma_T = 61 \pm 30$ deg) in the stimulus space centered on each unit's preferred motion. **B:** The preferred motion for each unit was selected randomly from a continuous estimate consistent with one of two preferred motion-pattern distributions reported in MST. The first, referred to here as unimodal, simulated the distribution of preferred motions biased toward expansions reported by Graziano et al. (1994). The second distribution, referred to here as bimodal, was similar in structure but contained a higher percentage of cells tuned to contracting motion patterns (Geesaman and Andersen, 1996).

population that serve to modify and refine the neural representation.

To examine this hypothesis, we constructed a population of MST-like units whose neural response properties were consistent with the reported physiology (Duffy and Wurtz, 1991a, 1991b; Geesaman and Andersen, 1996; Graziano et al., 1994; Orban et al., 1995) for cardinal and spiral preferred motion patterns (Fig. 4). For each neural unit, motion-pattern tuning followed a gaussian profile in the 2D stimulus space whose mean corresponded to the unit's preferred motion pattern. The standard deviation of each tuning profile was randomly selected from a uniform distribution (61 ± 30 deg), (Fig. 4A), consistent with the reported physiology for cardinal (62 ± 25 deg) and spiral (60 ± 34 deg) preferred motion cells (Graziano et al., 1994).

Within the model, simulations were categorized into one of three classes according to the underlying distribution of preferred motion patterns represented across the population (two reported in MST, Fig. 4B, and a uniform control). The first distribution simulated an anisotropy in which the density of preferred motion patterns decreased from expansions to contractions symmetrically across the motion-pattern space (Graziano et al., 1994). The second distribution was similar in structure but contained a higher percentage of cells tuned to contracting motion patterns (Geesaman and Andersen, 1996). The third distribution simulated a uniform preference for all motion patterns and was used as a control to examine the effects of an anisotropic distribution on perceptual performance. Throughout the article we refer to these preferred motion-pattern

distributions as unimodal, bimodal, and uniform, respectively.

For each physiological distribution of preferred motion patterns (unimodal and bimodal), probability density estimates $P(\phi)$ were obtained from the literature as a function of the flow angle (ϕ) using a three-parameter offset gaussian curve-fit of the form

$$P(\phi) = A_u + (1 - A_u) \times e^{-(\phi - \mu_g)^2/2\sigma_g^2},$$

where A_u is the amplitude of the offsetting uniform distribution, and μ_g and σ_g are the mean and standard deviation of the gaussian distribution, respectively. Least-square fits to the preferred motion distributions were obtained from normalized physiological population histograms that parsed the stimulus space into eight categories (radial, circular, and the four intermediate spiral motion patterns) (Zemel and Sejnowski, 1998). The resultant parameter estimates for A_u, σ_g, and σ_g ({0.15, 356.61 deg, 26.03 deg} and {0.34, 348.97 deg, 42.73 deg} for unimodal and bimodal distributions, respectively) were used to define the probability density of preferred motion patterns for each simulated population and randomly select the preferred motions of the (N) units in each population.

The visual motion response of each neural unit was represented as a steady-state estimate of firing rate combining motion-pattern responses with background noise averaged over some arbitrary time. Using the reported range of firing rates in MST (Duffy and Wurtz, 1991a, 1991b, 1995, 1997; Graziano et al., 1994; Orban et al., 1992), we estimated the average background and preferred motion firing rates to be 12 and 40 spikes/sec from samples of 23 and 51 cells, respectively. We assumed that the average preferred motion firing rates reported in the literature also incorporated background noise and estimated the mean preferred motion response to be 28 spikes/sec.

In MST, neural receptive fields typically span large regions of the visual field ($\sim$61 deg) (Duffy and Wurtz, 1991a, 1991b). For neurons preferring similar motion patterns, the resultant overlap in feed-forward visual input can introduce correlation into the neural output that varies with the relative spatial positions of the neural receptive fields. The structure associated with such correlations implies a redundant representation of neural information that can be used to aid information extraction across a population of noisy units. To simulate this effect in the model we assumed that units had comparable receptive fields such that neural responses

for similar preferred motions were moderately correlated ($r = [0.4, 0.8]$). Since the model did not explicitly contain a feed-forward layer of spatially localized inputs, we correlated neural responses by imposing a fixed maximum preferred response (R_{max}) across the population that varied as a Poisson process ($\lambda = 28$) for each stimulus presentation (Fig. 4A). The baseline neural output of each unit (N_i) was simulated as an uncorrelated Poisson process ($\lambda = 12$).

3.1.2. Model Structure. The psychophysical task was simulated across each neural population using a population vector to represent motion-pattern estimates in the 2D stimulus space (Fig. 1). A structural diagram of the model is shown in Fig. 5. Neural responses to the vector representations for each stimulus pair were calculated as an average firing rate (R_{av}) for the (ith) unit,

$$R_{av_i} = R_{\max} \times e^{-(\phi_N - \phi_i)^2/2\sigma_i^2},$$

where $R_{\max}$ is the maximum preferred stimulus response (spikes/s), ϕ is the motion pattern flow angle, and ϕ_i and σ_i correspond to the preferred motion pattern and tuning standard deviation of the ith unit, respectively. The net response (R_i) of each unit was formed by combining R_{av_i} with the baseline neural output (N_i).

For each stimulus, units voted for their preferred motion patterns with a weight equal to their net firing rate. The weighted response of each unit was represented as a vector in the unit's preferred motion direction, whose amplitude was a function of the unit's net response (R_i). Motion-pattern estimates were then decoded from the population as the population vector formed from the vector sum of responses across units.

Based on the population vector estimates obtained for each set of paired stimuli, the perceptual performance of the model was quantified using the negative perturbation ($-\phi_p$) discrimination of flow angle outlined in the psychophysical task. Discrimination thresholds were obtained from the population using a least-square fit to percent correct performance within a constant stimulus paradigm of motion pattern perturbation that matched the behavioral task.

In the first series of models, we quantified GMP discrimination across populations of independent neural units. For each class of models (unimodal, bimodal, and uniform), threshold performance was examined across five population sizes (100, 200, 500, 1,000, and 2,000 units). The range of discrimination thresholds and their
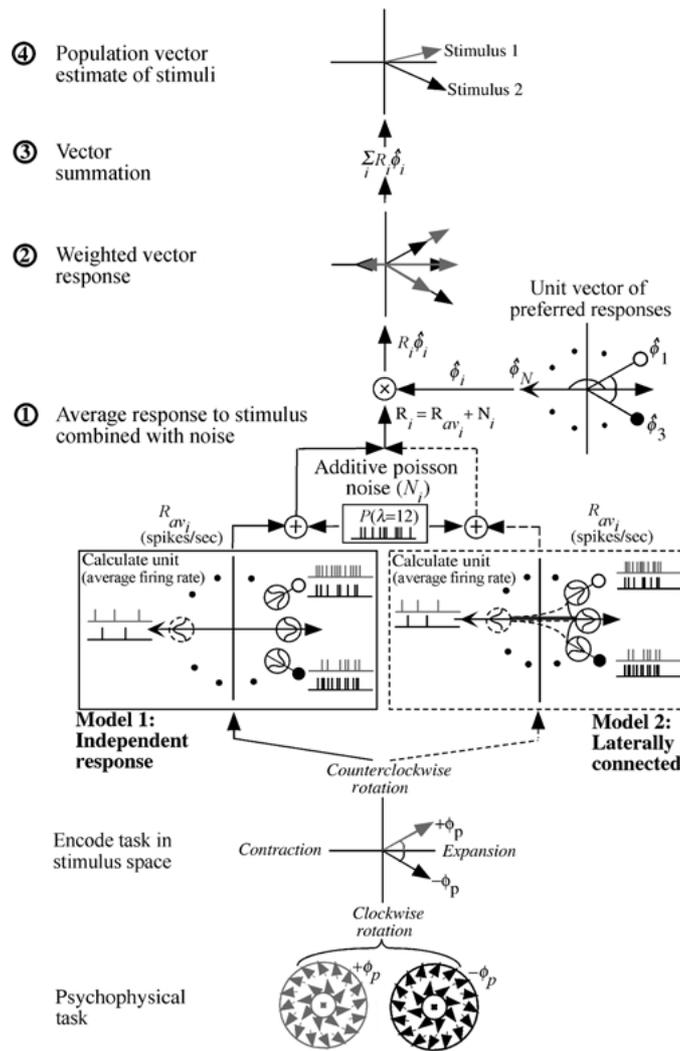
Figure 5. Schematic representation of the model structure. The psychophysical task was simulated using a population-vector representation of the motion patterns in the 2D stimulus space formed by coherent radial, circular, and spiral motions. For each stimulus, units voted (2) for their preferred motion with a weight equal to their net firing rate (1). In the stimulus space, the weighted response of each unit was represented as a vector in the unit's preferred motion direction. Stimuli were decoded from the neural representation as the population vector formed by the vector addition of the weighted responses across units (3). Using the psychophysical test protocol, was quantified "perceptual" performance based on the negative perturbation $(-\phi_p)$ discrimination of flow angle (4). Discrimination thresholds were obtained from the population using a least-square fit to percent correct performance within a constant stimulus paradigm of stimulus perturbation.

trends across test motions were compared across population sizes and model classes to assess which neural properties yielded motion-pattern discriminability that was quantitatively similar to human performance.

It is important to note that within this implementation the population vector does *not* provide an unbiased estimator of the motion-pattern flow angle (ϕ). The anisotropic distribution of preferred motion patterns introduces a bias into the vector representation

that is skewed toward expanding motion patterns. As a result, increasing populations do not yield vector representations that converge to the proper 2D motion pattern. This makes accurate interpretation of the individually decoded stimuli problematic without *a priori*–knowledge of the nonlinear transformation associated with the bias in the vector representation.

To compensate for this, the model's performance was based on the relative spatial locations *between* the pairs

of motion patterns presented in the 2TAFC task and not the proper 2D spatial location of each decoded motion pattern. In this way, the population vector could assume any smooth nonlinear mapping without imposing *a priori* assumptions regarding the underlying transformation and thus was not constrained to linearly map the stimulus space onto the internal neural representation.

3.1.3. Lateral Connections Between Units.

In a second series of models, we examined the computational effect of adding lateral connections between neural units. If the distribution of preferred motion patterns in MST is in fact anisotropic, as the physiology suggests, it seems unlikely that independent estimates of the visual pattern information would be sufficient to yield the perceptual profiles obtained in the psychophysical task. We hypothesize that a simple fixed architecture of excitatory and/or inhibitory lateral connections between neural units is sufficient to yield the observed perceptual trends in the presence of an anisotropic preferred motion distribution biased toward expanding motion patterns.

In the models proposed here, neural units were fully interconnected with fixed excitatory and/or inhibitory connections. Within this architecture, each neural response consisted of the summed output from three nonlinear transfer functions corresponding to (1) the incident visual motion pattern, (2) internal neural noise (not associated with the motion pattern), and (3) a modulating lateral input (Fig. 6).

In each simulated population, the strength of the individual connections varied as a function of the similarity in preferred motion patterns between neural units. Using the flow-angle representation for preferred motion patterns, excitatory connections from the ith unit (with preferred motion ϕ_i) were made to units with similar preferred motions (Fig. 7a). The strength of excitation followed a gaussian profile centered around ϕ_i with a fixed standard deviation (σ_E) across the population. Similarly, units with antipreferred motions received inhibitory connections whose strength followed a gaussian profile centered around $180 + \phi_i$. To examine the effects of inhibitory spread and connection strength in the model, the standard deviation of gaussian inhibition (σ_I) and level of excitatory/inhibitory activity (S_A) were considered free parameters.

For each unit, the level of excitatory and inhibitory activity followed a nonlinear postthreshold increase proportional to the firing rate. When a unit's response exceeded a fixed threshold ($T_I = 28$), its contributed
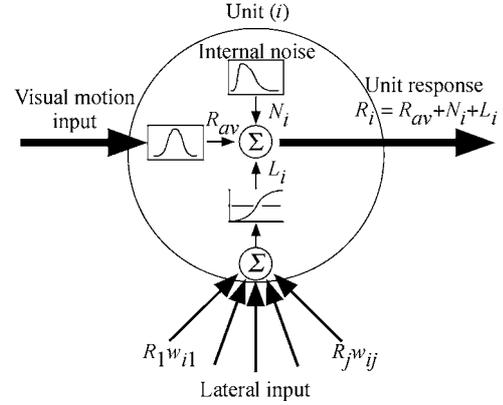

Figure 6. Input-output diagram for unit (i). The response of each neural unit was formed from the summed combination of visual motion input and internal noise represented as average firing rates (spikes/s). Visual motion responses were generated as a function of the euclidian distance between each unit's preferred motion vector and the 2D vector representation of the motion pattern. Internal noise was simulated as an uncorrelated Poission process ($\lambda = 12$). When lateral interactions were simulated within the population, each unit received a third input formed by the nonlinear postthreshold summation of the weighted input from all incident lateral connections.

lateral activity to the population was calculated by scaling its response with the activity parameter (S_A) and the weighted connection to each unit. The resulting level of excitatory/inhibitory activity (L_i) contributing to the ith unit's response was calculated using a nonlinear sigmoid function of the form

$$L_i = \left[\frac{2}{1 + e^{\frac{-S_A \sum_j w_{ij} R_{tj}}{35}}} - 1 \right] \times 20;$$
$$R_{tj} = 0, \quad R_i \leq 28$$
$$= R_i, \, otherwise,$$

where R_{tj} is the response of the jth postthreshold unit, w_{ij} is the normalized lateral weight between the ith and jth units, and S_A is the strength of lateral activity (Fig. 7B). Across the population, L_i spanned a ± 20 spike/sec range over an integrated input ($S_A \sum_i w_{ij} R_{ti}$) of ± 120 spikes/sec and was used to modulate each unit's motion pattern response over the range of observed physiological firing rates (0 to 70 spikes/s). Negative spike rates associated with large inhibitory inputs were rectified to a zero bound prior to calculating the population vector used in the discrimination task.

In each model class (unimodal, bimodal, and uniform) the simulated perceptual performance across the
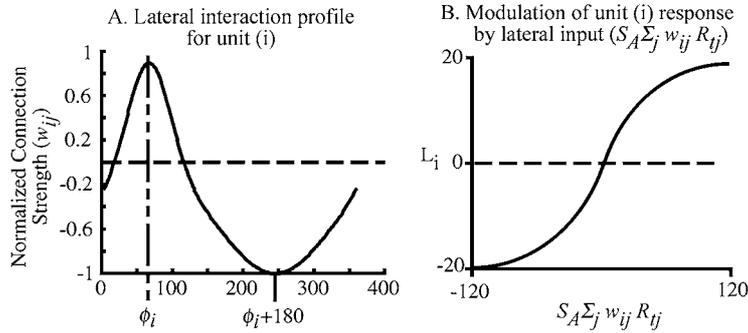
Figure 7.   Lateral connection profiles between units. **A:** A Cartesian representation of the normalized connection weights projected from unit (*i*), with preferred motion (ϕ_n), in the laterally connected model. Using the stimulus vector representation for preferred motion patterns, excitatory connections from the *n*th unit (with preferred motion ϕ_n) were made to units with similar preferred motions. The strength of excitation was normally distributed around ϕ_n with a standard deviation (σ_E) that could be varied across simulations. Units with antipreferred motions received inhibitory connections whose strengths were normally distributed around the anti-preferred motion ($180 + \phi_n$) with standard deviation σ_I. Throughout the simulations σ_I and the level of excitatory/inhibitory activity (S_A) were considered free parameters. **B:** The level of excitatory and inhibitory lateral modulation of each unit was calculated using a nonlinear postthreshold function proportional to the firing rate. When a unit's response exceeded a fixed threshold ($=28$), its lateral interaction within the population was calculated by scaling its average firing rate with the weighted connections ($S_A w_{ij}$) to other units. The total lateral input to each unit was passed through a saturating nonlinearity (range of ± 20 spikes/sec) and was used to modulate the original stimulus response over the range of observed physiological firing rates (0 to 70 spikes/s). Negative spike rates associated with large inhibitory inputs were rectified to zero.

population was examined over a range of σ_I and S_A ([5 to 150 deg] and [0.1 to 10], respectively). For each parameter combination, discrimination thresholds were correlated with the equivalent psychophysical thresholds to estimate the range of σ_I and S_A over which the population code was consistent with human performance. Model performance was also quantified as a coarse function of the spread of excitatory connections by examining the resulting (σ_I, S_A) correlation maps across four levels of σ_E (20, 30, 45, and 60 deg).

3.1.4. Neural Response Thresholds.   In a third series of models we examined the effect of imposing a threshold on the unit responses contributing to the population vector. Here, neural responses were multiplied with a Heaviside function $H(T_R)$ that rectified subthreshold (T_R) responses to zero prior to weighting the unit's preferred motion vector:

$$H(T_R) = 0, \qquad R_i \leq T_R$$
$$= 1, \qquad R_i \geq T_R.$$

The simulated perceptual performance of each model class was examined over a range of rectifying thresholds ($T_R = [1, 61]$ spikes/sec). Similar to the previous implementations, the model's performance was correlated with the psychophysical thresholds to estimate the range of T_R over which the population

code was consistent with human performance. Threshold performance was then examined as a function of population size for each of the three model classes (unimodal, bimodal, and uniform) using an optimal T_R selected from the composite regions of highest correlation.

3.2.   Results

3.2.1. Discriminating Motion Patterns in a Population Code of Independent Neural Responses.   For each class of models (unimodal, bimodal, and uniform), discrimination thresholds were averaged across a minimum of five independently generated populations in an effort to reduce the effects of discrete statistical variations in the distributions of simulated preferred motion pattern. Discrimination thresholds for these independent-response populations showed extensive variability as a function of their population size and distribution of preferred motion patterns (Fig. 8). While the models' performance was generally comparable to the psychophysical thresholds for expansions and expanding spiral motion patterns, thresholds for contracting motions consistently and significantly exceeded human performance even for the largest populations.

Discrimination thresholds for unimodal populations were inconsistent with psychophysical results across

Figure 8. Psychophysical performance of the independent-response models averaged across five simulated populations. GMP discrimination thresholds (±1 standard error) showed extensive variability as a function of the population size and the distribution of preferred motion patterns. **A:** Across all population sizes, unimodal thresholds were highest for contracting motions and lowest for expanding motions. Over the psychophysical range of interest ($\phi \pm 7$ deg), discrimination thresholds for contracting motions were at chance while thresholds for circular motion patterns remained significantly higher than those reported in the psychophysical task. **B:** Bimodal discrimination thresholds were more consistent with human performance particularly for moderately large populations (>1,000 units). With increasing population size discriminability for contraction motion patterns ($\phi = 180$ deg) steadily decreased to levels observed for expansions ($\phi = 0$ deg). However, even for the largest populations discriminability for contracting spiral motions remained poor. **C:** Across uniform models, designed to control for the effects of the underlying preferred motion-pattern distribution, the range of discrimination thresholds was generally consistent with human performance. However, with the exception of the 100-unit population average the flat trend in thresholds across motion patterns did not approximate the sinusoidal trend observed psychophysically.

both stimuli and population sizes. Over the psychophysical range of interest ($\phi \pm 7$ deg), discrimination thresholds for contracting motions were at chance across all populations (100 to 2,000 units) while thresholds for circular motion patterns remained significantly higher than those reported in the psychophysical task (Fig. 8a). Across the eight psychophysical test motions, discrimination thresholds showed no significant improvement with increasing population size.

Discrimination thresholds for bimodal populations were more consistent with human performance,

particularly as population size increased. Contraction ($\phi = 180$ deg) thresholds for larger populations steadily decreased to those obtained for expansions ($\phi = 0$ deg) (Fig. 8b); however, even for the largest populations discriminability for contracting spiral motions remained poor.

Unlike the unimodal populations, the performance of bimodal populations also improved asymptotically with population size across test motions. This was particularly true for contractions ($\phi = 180$ deg), which decreased six-fold for a 20-fold increase in popula-

tion size. While this decrease in perceptual thresholds did make the overall range of performance more comparable with human discriminability, the independent-response bimodal populations remained unable to accurately reproduce human performance in the asymptotic limit observed through 2,000 units.

In simulations containing a uniform distribution of preferred motion patterns, designed to control for the effects of an anisotropic distribution, the range of discrimination thresholds was consistent with human performance. However, with the exception of the averaged 100-unit performance, the trend in thresholds across motion patterns was flat. Closer inspection of the 100-unit threshold variations shown in Fig. 8C together with the corresponding preferred motion-pattern distributions suggested the observed variability arose in large part due to the discrete sampling of the uniform preferred motion probability density function. In subsequent simulations (not shown here), more extensive threshold averaging across 10 simulations reduced the observed variability, resulting in threshold profiles that were well fit by a line whose slope was near zero.

Further inspection of the pooled neural information across model classes suggests that the variability in threshold performance observed across test motions resulted primarily from the combined effect of the background noise and the population biases for expanding motion patterns. For nonexpanding motion pattern subpopulations, such as those preferring contractions, the proportion of units responsive to a nonexpanding stimulus was typically a small percentage of the total population. In these cases, the population vector contained a significant degree of noise associated with the nonpreferred background response vector summed across large populations of expansion preferred units—that is, signal-to-noise ratio (SNR) < 1. As population size increased, the nonuniform effect of the preferred motion anisotropy on the population SNR (across test motions) caused discrimination thresholds to closely track the degree of preferred motion bias within each model class. When the population SNR was less than one, increases in population size further increased the net vector contribution of noise, decreasing the SNR, and severely impairing discrimination (such as unimodal populations). Similarly, when the SNR was greater than one, increases in population size asymptotically increased the SNR and decreased perceptual thresholds (for example, bimodal populations).

3.2.2. Effects of Excitatory and Inhibitory Lateral Connections Between Units.

Within the structural parameter space used to define lateral activity between units—that is, strength (S_A) and spread (σ_I, σ_E)—both the overall level of GMP threshold performance and the trend across test motions varied widely for the ranges of parameters examined. Monte Carlo simulations across the three-dimensional parameter space yielded regions of high correlation (with respect to the psychophysical thresholds) that were consistent across independently simulated populations for unimodal and bimodal model classes. Typically, these regions were well defined over a wide but limited range of σ_I and S_A. Figure 9 illustrates this result for averages of five unimodal and eight bimodal populations containing 200 units each ($\sigma_E = 30$ deg). In both cases the regions of best correlation (80% of maximum) were generally robust, extending over a broad range of σ_I [60, 120 deg] and S_A [0.15, 0.5].

While the maximum level of correlation within these regions typically accounted for only a fraction of the psychophysically observed variance across motion patterns (25 to 50%), comparable simulations with populations of 100 units indicated an increasing trend in correlation as a function of population size. Unimodal and bimodal populations of 100 units showed similar regions of correlation—σ_I (70, 120 deg) and S_A [0.2, 5]—that were well matched to those observed across 200 unit populations. Although the ranges of values reported here for S_A decrease with increasing population size, it is important to note that the overall level of lateral activity implied by these ranges is similar for the two population sizes. Additional simulations that varied the spread of excitation (σ_E) showed comparable regions of correlation that were robust across the range of σ_E examined [20, 60 deg].

Unlike the physiological distributions of preferred motion patterns, Monte Carlo simulations of uniform population distributions did not yield consistent regions of psychophysical correlation. For 100-unit populations the averaged correlation plot was flat ($r = 0 \pm 0.2$). Simulations using 200 units showed more variation across the parameter space and exhibited a small region of significant correlation ($r \sim 0.5$) over the range $\sigma_I = [100, 120$ deg] and $S_A = [0.1, 0.3]$ but remained uncorrelated with human performance.

Although these results suggested that larger populations would yield regions of increasingly higher correlation, the computational cost imposed by these larger simulations precluded an exhaustive search of the
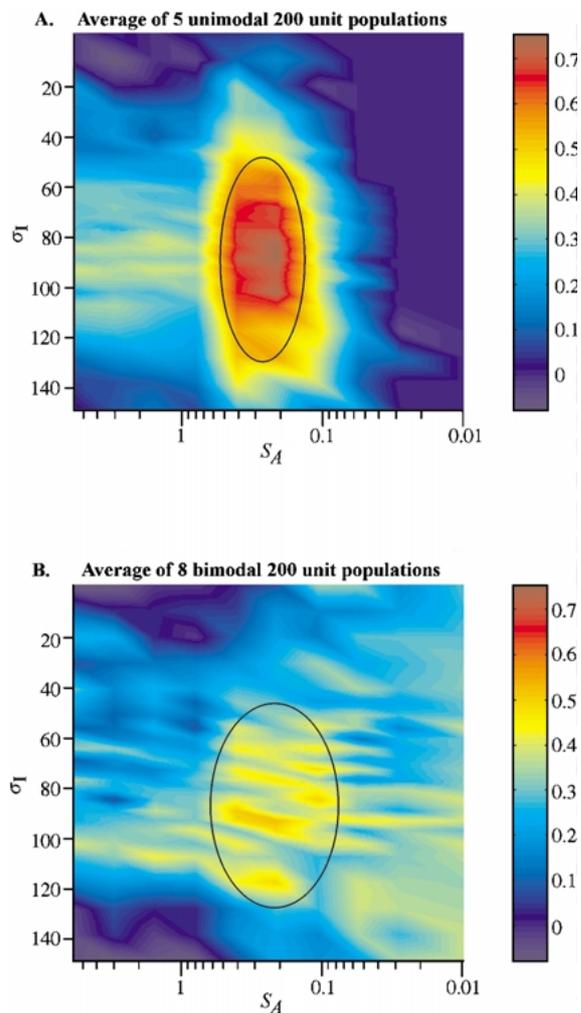
Figure 9. Discrimination thresholds of the laterally connected model correlated with the psychophysical performance as a function of the strength of excitatory/inhibitory activity (S_A) and the spread of inhibitory connections (σ_I). The averaged performance of each simulation was correlated with psychophysical GMP thresholds across a minimum of five 200-unit populations using a fixed spread of excitatory connections ($\sigma_E = 30$ deg). For unimodal/bimodal populations the regions of interest (ROI) denoted by the black contours ($\geq 80\%$ of maximum correlation) were generally robust extending over a broad range of σ_I [60, 120 deg] and S_A [0.15, 0.5]. While the maximal level of correlation within these regions typically accounted for only a fraction of the psychophysically observed variance (25 to 50%), comparable simulations with populations of 100 units indicated an increasing trend in the level of correlation as a function of poputltation size. To extend simulations to larger populations, optimal values for σ_I and S_A were estimated based on the ROI centroid. Across models, centroid estimates for σ_I were generally independent of σ_E. Using a fixed σ_E (=30 deg), 200-unit centroid estimates of [$\sigma_I = 88$ deg, $S_A = 0.37$] and [$\sigma_I = 91$ deg, $S_A = 0.36$] were obtained for the unimodal and bimodal models, respectively.

parameter space for populations of more than 200 units. To offset this limitation, we confined the simulations of larger populations to a set of optimal structural parameters estimated from the highly correlated regions of interest (ROI) corresponding to 80% of maximum correlation.

Within this region, optimal values for σ_I and S_A were estimated from the ROI centroid[1] which was generally independent of σ_E across models. Using a fixed σ_E (=30 deg), 100-unit centroids of [$\sigma_I = 106$ deg, $S_A = 1.77$] and [$\sigma_I = 76$ deg, $S_A = 1.93$] and 200-unit centroids of [$\sigma_I = 88$ deg, $S_A = 0.37$] and [$\sigma_I = 91$ deg, $S_A = 0.36$] were obtained for unimodal and bimodal models, respectively. For smaller values of σ_E (<30 deg), σ_I centroid estimates decreased across models by approximately 8 deg.

Based on the centroids estimated from the 100-unit correlation maps we selected optimal values of σ_I and S_A for use in simulations of larger populations. Given the lack of significant correlation across uniform populations and the similarities in centroids for the unimodal and bimodal populations, we set the optimal 100-unit σ_I and S_A to 80 deg and 1.5, respectively. For larger populations the connection strength (S_A) was scaled inversely with the population size to maintain an equivalent level of lateral activity and facilitate a comparative analysis across populations.

Figure 10 shows the averaged threshold performance across model classes for three population sizes (100, 500, and 2,000 units). The incorporation of lateral connections between units significantly decreased the range of discrimination thresholds to psychophysically observed levels. More important, as population size increased the sinusoidal trend in threshold performance observed across test motions began to emerge for both the unimodal and bimodal models. The threshold trends across test motions were well established for as few as 500 units and were well fit ($r > 0.9$) by sinusoids whose periods and phases were (173.7 ± 6.9 deg, −67.21 ± 16.78 deg) and (208.3 ± 10.2 deg, −60.68 ± 15.74 deg) for the unimodal and bimodal populations, respectively. These results are in good agreement with the fitted psychophysical trend shown here for SB (196.6 ± 12.8 deg, −75.27 ± 23.42 deg).

Unlike the unimodal/bimodal model classes, Uniform population distributions were not significantly affected by the presence of lateral connections. The range of thresholds were typically well matched to the independent-response uniform simulations and asymptotically decreased well below perceptual thresholds
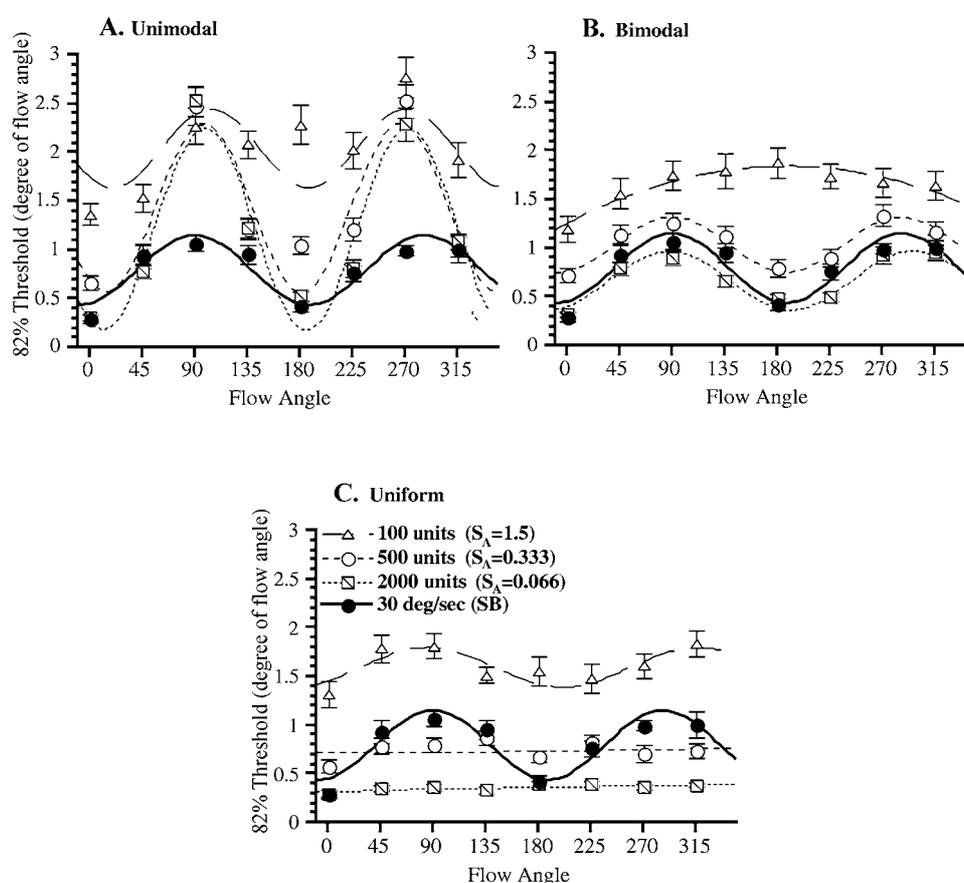
Figure 10. Psychophysical performance of the laterally connected model with excitatory and inhibitory lateral connections between units. Performance was averaged across five simulated populations with $\sigma_I = 80$ deg, $\sigma_E = 30$ deg, where the strength of lateral activity (S_A) was scaled to maintain a consistent level of lateral input with increasing population size. As the population size increased, discrimination thresholds decreased to psychophysical levels and the sinusoidal trend observed across motion patterns began to emerge for both the **(A)** unimodal and **(B)** bimodal model classes. Sinusoidal trends were established for as few as 500 units and were well fit ($r > 0.9$) by sinusoids whose periods and phases were (173.7 ± 6.9 deg, −67.21 ± 16.78 deg) and (208.3 ± 10.2 deg, −60.68 ± 15.74 deg) for the unimodal and bimodal models, respectively. These results are in good agreement with the fitted psychophysical trend (196.6 ± 12.8 deg, −75.27 ± 23.42 deg). **C:** Unlike the unimodal/bimodal populations, the uniform model was not significantly affected by the presence of lateral connections. Here the averaged 100-unit thresholds contain variations across motion patterns similar to the observed psychophysical trend. However, thresholds for larger populations became increasingly more uniform, suggesting the presence of discrete statistical fluctuations that were not completely cancelled in the average across independent populations.

for moderately large populations (~2,000 units). While the averaged 100-unit thresholds did contain variations across test motions that were similar to the psychophysical trend, thresholds for larger populations became increasingly more uniform, suggesting the presence of discrete statistical fluctuations that were not cancelled out in the average across multiple simulations.

Closer inspection of the uniform model 200-unit performance within the structural parameter ROI showed similar trends in performance. For optimal ROI values of σ_I (=110 deg) and S_A (=0.2), discrimination thresholds across motion patterns were approximately constant at 1 deg. In this case the model performance captured the variance associated with the perceptual thresholds for expanding spiral and circular motion patterns without accurately approximating the sinusoidal trend. Simulations of larger uniform populations, with $\sigma_I = 110$ deg and S_A scaled to maintain a consistent level of lateral activity, continued to deviate from the psychophysical trend and were well matched to the flat threshold distributions shown in Fig. 10C for 500 and 2,000 units.
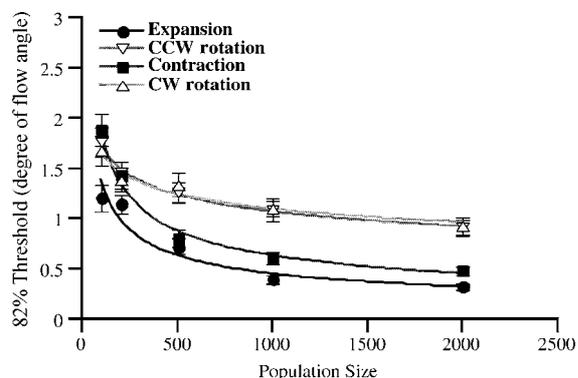
Figure 11. Discrimination thresholds of the bimodal model as a function of population size for cardinal test motions (radial and circular). The decrease in thresholds followed an inverse power law whose exponent varied as a function of the test motion pattern over a broad range [0.05, 0.5]. Across all test motions the threshold slope decreased quickly with population size such that for 2,000 units the change in threshold was 0.008 deg for each 100 unit increase in the population. Comparable performance was obtained across all test motions and model classes (unimodal, bimodal, and uniform).

Throughout the unimodal and bimodal simulations presented here, threshold performance decreased asymptotically with increasing population size for all test motion patterns. An example of the averaged cardinal motion (radial and circular) thresholds for the bimodal model is shown in Fig. 11. The decrease in thresholds followed an inverse power law whose exponent varied as a function of the test motion pattern across an order of magnitude [0.05, 0.5]. For all test motion patterns the threshold slope decreased quickly with population size such that for 2,000 units the change in threshold performance was 0.008 deg for each 100 unit increase in the population. Together with the computational robustness to large variations in the underlying neural properties (that is, populations size and the distribution of preferred motions) obtained here these results make this form of highly interconnected architecture appealing as a method for encoding visual motion information consistently across a neural population.

3.2.3. Effects of Thresholding Neural Responses.
While the addition of lateral interactions between units does provide discrimination thresholds that are in good agreement with human performance, it does not preclude other methods of noise reduction within the neural structures used to extract perceptually relevant measures of discrimination. When threshold population vector estimates were based on a subset of

thresholded (T_R) neural responses obtained from an independent-response neural architecture, the resulting discrimination profiles obtained across motion patterns and population sizes were found to be similar to laterally connected models containing extensive excitatory/inhibitory lateral connections between units.

Simulations of GMP discrimination across a range of rectifying threshold values ($T_R = [0, 60]$ spikes/s) contained regions that were significantly correlated with human performance in each of the three model classes. In 100-unit threshold populations, discrimination thresholds were correlated for T_R values ranging from 30 to 50 spikes/s. Similar regions of correlation were obtained for 200-unit populations (Fig. 12) over a slightly larger range (20 to 50 spikes/s). ROI estimates of the T_R centroid across each of these conditions yielded a composite estimate of 35 spikes/s that was subsequently used to examine performance as a function of population size.

Figure 13 illustrates the averaged thresholds for the unimodal, bimodal, and uniform model classes across three population sizes (100, 500, and 2,000 units) when $T_R = 35$ spikes/s. With this level of T_R imposed prior to calculating the population vector, the range of discrimination thresholds decreased significantly to psychophysically observed levels for moderate population sizes. Similar to the laterally connected unimodal/bimodal models, increases in population size increased the sinusoidal trend in threshold performance obtained across test motions. Here the perceptual trends across test motions were established for 1,000 units and were well fit ($r > 0.85$) by sinusoids whose periods and phases were (218.5 ± 15.7 deg, -37.98 ± 21.35 deg) and (216.9 ± 21.9 deg, -42.17 ± 30.34 deg) for the unimodal and bimodal models, respectively.

In contrast, simulations of threshold uniform populations indicated a *decrease* in discriminability as compared to the independent response simulations shown in Fig. 8C. For 100-unit populations, the range of discrimination thresholds (2 to 4 deg) was significantly higher than that obtained previously without the use of a T_R (1 to 2 deg) (Fig. 13C). While the level of discriminability remained significantly higher across population sizes for threshold populations, the overall trend was well matched to the independent response uniform model. Like the independent response simulations, performance quickly became flat across test motions and asymptotically decreased well below the level of perceptual thresholds for large populations (>2,000 units).
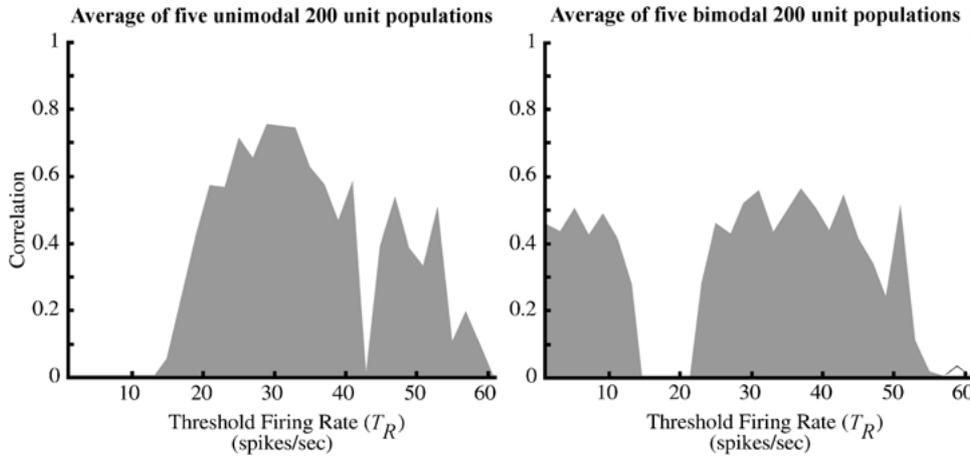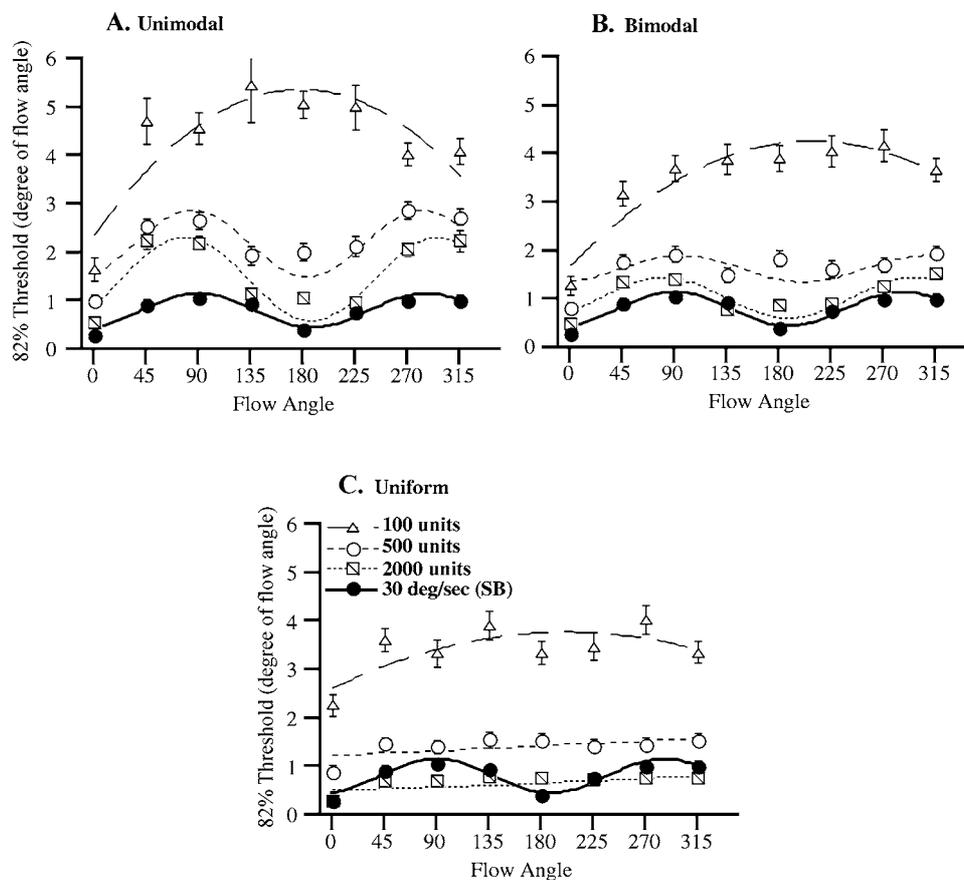
Figure 12. Threshold model performance as a function of an intrinsic rectifying threshold (T_R) applied prior to estimating the population vector. Discrimination thresholds were correlated with human psychophysical performance across the eight test motions. Simulations of GMP discrimination across a range of threshold values ($T_R = [0, 60]$ spikes/s) contained regions that were significantly correlated with human performance for all three model classes. GMP discrimination for 200-unit populations was significantly correlated for T_R values ranging from 20 to 50 spikes/s. ROI estimates of the T_R centroid across model classes and population sizes (100 and 200 units) yielded a composite optimal T_R estimate of 35 spikes/s.

A closer examination of the response characteristics within the threshold unimodal/bimodal models examined here indicates that the proportion of units responding consistently above threshold (>80% of the time) varied with the test motion pattern, from a low of 1.4% for contractions to a high of 11% for expansions (unimodal populations) (Table 1). The subsequent exclusion of minimally responsive units, due to response thresholding, reduced the variability of the predicted motion pattern in a manner consistent with the presence

Table 1. Proportion of neural units consistently responding to radial motion patterns in the threshold unimodal and bimodal models ($T_R = 35$ spikes/s). The proportion of units responding consistently above threshold (>80% of the time) varied with the motion pattern, from a low of 1.4% for contractions to a high of 11% for expansions (unimodal populations). The range of preferred responses for units responding above threshold was generally constant across models and motion patterns. In both model classes, the proportion of units contributing to the population vector varied as a function of the test motion pattern and typically comprised a fraction of the total population.

|	Unimodal			
	Expansion		Contraction	
Units responding	Proportion	Range of pref. resp.	Proportion	Range of pref. resp.
>80% of the time	11.2%	53 deg	1.4%	37 deg
>60% of the time	34.4%	82 deg	6.5%	85 deg
	Bimodal			
	Expansion		Contraction	
Units responding	Proportion	Range of pref. resp.	Proportion	Range of pref. resp.
>80% of the time	8.2%	54 deg	3.8%	48 deg
>60% of the time	27.0%	94 deg	12.4%	71 deg

Figure 13. Psychophysical performance of threshold models containing an intrinsic rectifying threshold. Performance was averaged across five simulated populations with $T_R = 35$ spikes/s. The range of discrimination thresholds decreased significantly, relative to independent-response simulations, to psychophysically observed levels for moderately sized populations. Increases in population size increased the sinusoidal trend in threshold performance observed across motion patterns. Equivalent perceptual trends were well established for 1,000 units and were well fit ($r > 0.85$) by sinusoids whose periods and phases were (218.5 ± 15.7 deg, -37.98 ± 21.35 deg) and (216.9 ± 21.9 deg, -42.17 ± 30.34 deg) for the (**A**) unimodal and (**B**) bimodal models, respectively. **C:** Simulations of threshold uniform populations indicated a *decrease* in discriminability as compared to the independent-response simulations shown in Fig. 8C. For 100-unit populations, the range of discrimination thresholds (2 to 4 deg) was significantly higher than that obtained previously *without* the use of a T_R (1 to 2 deg). As the population size increased, threshold performance became flat across motion patterns and asymptotically decreased well below perceptual thresholds for large populations ($>2,000$ units).

of inhibitory lateral connections between antipreferred motion pattern units. As a result, for unimodal and bimodal models in particular, the proportion of units contributing to the population vector varied as a function of the test motion and typically comprised only a small fraction of the total population. Such performance is generally consistent with a winner-take-all strategy of neural coding and the pre-synaptic inhibitory architecture it implies (Haykin, 1999; Hertz et al., 1991).

3.2.4. Effects of Inhibitory Lateral Connections Between Units.
The development of a sinusoidal trend

in GMP discrimination for large threshold populations ($>1,000$ units), together with the inhibitory winner-take-all structures implied by their sparse coding, suggest that similar performance could be obtained from populations containing *only* inhibitory lateral connections between units. Although early simulations using small populations to search for regions of significant correlation across the (σ_I, S_A) parameter space were inconclusive, the inability of small threshold models to reproduce the psychophysical trend suggests that larger populations might be required to significantly increase the signal-to-noise ratio of the system. Using the
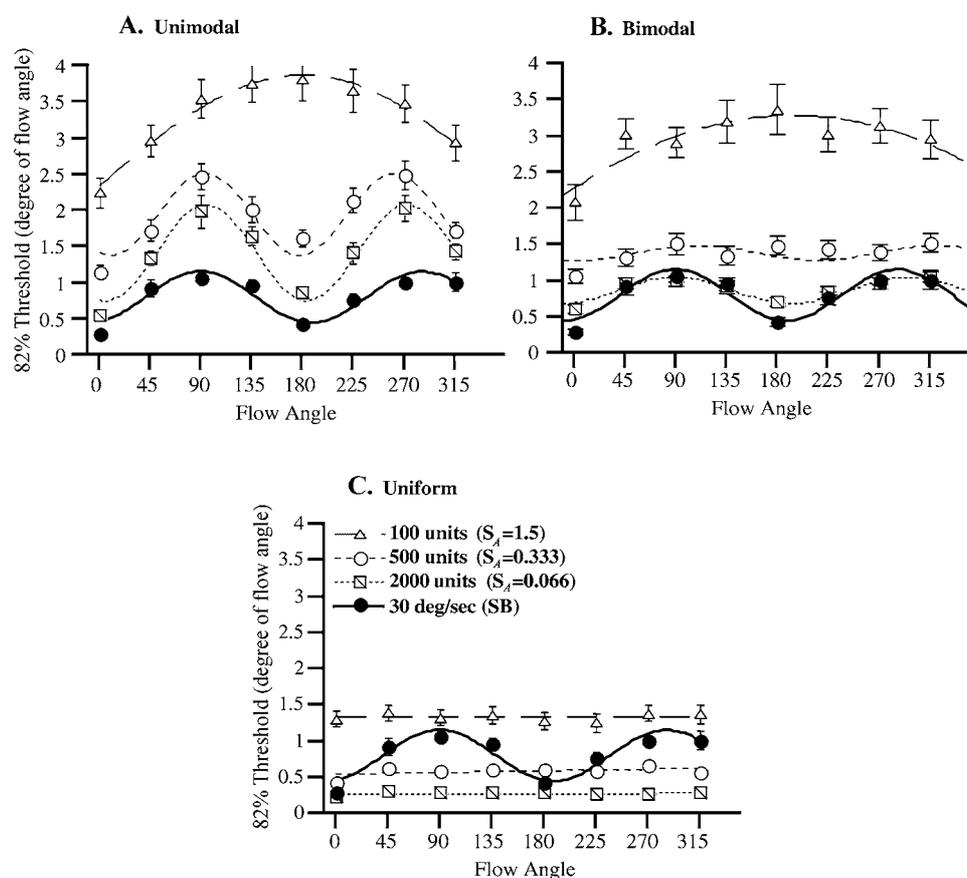
Figure 14. Psychophysical performance of laterally connected models with inhibitory lateral connections between units. Performance was averaged across five simulated populations with $\sigma_I = 80$ deg and where the strength of lateral activity (S_A) was scaled to maintain a consistent level of lateral input across population sizes. As population size increased the sinusoidal trend obtained in the psychophysical task began to emerge for (**A**) unimodal and (**B**) bimodal models. The trends were established for 1,000 units and were well fit ($r > 0.9$) by sinusoids whose periods and phases were (178.0 ± 6.0 deg, −79.48 ± 13.93 deg) and (205.8 ± 16.2 deg, −65.77 ± 25.88 deg) for the unimodal and bimodal models, respectively. (**C**) As with previous uniform simulations, the range of discrimination thresholds was consistent with human performance; however, the trend across motion patterns remained flat.

optimal structural parameters obtained previously from the laterally connected models containing excitation and inhibition, we examined discrimination thresholds for mutually inhibiting populations of up to 2,000 units (Fig. 14).

With the addition of inhibitory lateral connections, the discrimination thresholds for large populations asymptotically approached those obtained using laterally connected architectures of excitatory *and* inhibitory interactions. As the population size increased, the sinusoidal trend obtained across test motions began to emerge for both the unimodal and bimodal models. Typically the perceptual trends were established for 1,000 units and were well fit ($r > 0.9$) by sinusoids whose periods and phases were (178.0 ± 6.0 deg,

−79.48 ± 13.93 deg) and (205.8 ± 16.2 deg, −65.77 ± 25.88 deg) for the unimodal and bimodal models, respectively. These results are in good agreement with both the fitted psychophysical trends and the performance of the laterally connected excitatory/inhibitory models for moderate population sizes (∼500 units).

As with the excitatory/inhibitory architecture simulated previously, the discrimination thresholds of models containing *only* inhibitory connections decreased asymptotically with increases in population size. Subsequent simulations for even larger populations (∼5,000 units) showed little change in the threshold amplitudes or their trends across test motions and model classes. Similarly, the computational performance of the large laterally connected inhibitory neu-

ral populations was also consistent with the trends in human perceptual performance and was robust to variations in the underlying distribution of preferred motion patterns. Together with the robust encoding of motion-pattern information obtained across σ_E, these results indicate that psychophysical performance in the GMP discrimination task may be mediated primarily through signal enhancement associated with the strength and spread of inhibitory lateral connections.

4. Discussion

The graded motion pattern (GMP) discrimination task presented here (see also Beardsley and Vaina, 2001) indicates that human discrimination varies consistently with the pattern of complex motion over a range of thresholds ($\phi = 0.5$ to 2 deg). For each observer, the trend in perceptual thresholds across motion patterns consistently demonstrates a preference for radial motions that is qualitatively similar to the bias for expanding motions reported in the medial superior temporal area (MST) of nonhuman primates. Together with the preferences for global motion patterns reported in MST, these results suggest that much of the perceptual information, if not the underlying neural circuitry, involved in the discrimination of motion patterns may be represented in the human homologue to MST.

Using biologically plausible neural units we have shown that the motion information encoded in the activity of a population of MST neurons is sufficient to obtain discrimination thresholds consistent with human performance. Theoretically, the computations required to perform the perceptual task can be obtained by comparing the nonzero responses between pairs of motion pattern cells that adequately span the 2D stimulus space. However, in practice neural populations are typically required to extract the desired visual motion information given the presence of neural noise not associated with the stimulus and the lack of *a priori* knowledge concerning the variability in stimulus tuning profiles across cells.

In the neural populations simulated here, the 2D stimulus representation facilitated the choice of a population vector decoding strategy to extract perceptually meaningful motion-pattern information. With this implementation, the physiologically reported anisotropic distribution of preferred motion patterns in MST introduced a computational bias in the vector estima-

tion of the flow angle (ϕ) that was skewed toward expanding motion patterns. Under these conditions, increases in population size did not yield vector representations that converged to the proper 2D motion pattern, making accurate interpretation of individually decoded stimuli problematic without *a priori* knowledge of the nonlinear transformation associated with the bias.

To compensate for this, the model's performance was based on the relative spatial locations *between* the pairs of motion patterns presented in the 2TAFC task and not the proper 2D spatial location of each decoded motion pattern. In this way, the population vector could assume any smooth nonlinear mapping without imposing *a priori* assumptions regarding the underlying transformation and thus was not constrained to linearly map the stimulus space onto the internal neural representation.

While sufficient for the psychophysical task outlined here, this limitation in the decoding strategy restricts the model's general application to perceptual tasks consisting of single-interval stimulus presentations. This deficiency could be overcome using computationally more robust decoding schemes such as Bayesian inference (Oram et al., 1998) and probability density estimation (Sanger, 1996; Zemel et al., 1998) that do not require an explicit representation of the stimulus space. Within such decoding schemes the addition of lateral inhibitory connections, while mathematically more complex, would seem likely to affect discriminability in comparable ways by minimizing the stimulus uncertainty associated with the overlap of probability distributions within a multidimensional neural representation.

Similar but less extreme conditions may also occur in models of free arm reaching (Georgopoulos et al., 1986, 1988; Lukashin and Georgopoulos, 1993, 1994; Lukashin et al., 1996) for which the monkey physiology suggests the presence of statistically significant deviations from uniformity in both motor cortex (Schwartz et al., 1988) and parietal area 5 (Kalaska et al., 1983). Within each of these models there has been an implicit assumption of uniformity in the neural representation that, in the asymptotic limit of increasing population size, predicts that population vector estimates will converge to the proper reaching vector representation. However, if this uniformity assumption is not met, as in the model we have presented, the theoretical convergence breaks down in proportion to the degree of nonuniformity and the locations of stimulus vectors

relative to the bias. Depending on the actual degree of anisotropy within cortical motor areas, asymptotic reaching errors such as those reported by Georgopoulos et al. (1988) might in fact be artifacts associated with an underlying nonuniformity in the 3D reaching representation.

4.1.   Discriminating Motion Patterns in a Population Code of Independent Neural Responses

Under physiological conditions consistent with the visual motion responses of cells in MST, we have demonstrated that the population vector information decoded from independently responding neural units *is not* computationally sufficient to extract perceptual estimates that are consistent with human performance. For anisotropic neural populations containing a strong preferred motion bias for expanding motion patterns (unimodal and bimodal models), large amounts of noise were introduced into the population vector estimate for nonexpanding stimuli. In the extreme case of contracting motions, only 20% of the population typically responded to the stimulus. For those units that responded significantly, the encoded signal-to-noise ratio (SNR ≈ 2) was typically offset by a significantly larger vector contribution of noise encoded across the population (SNR $\ll 1$). This introduced considerable variability in the motion pattern estimates and causes discrimination thresholds to increase.

In contrast, the independent-response uniform models were able to approximate the psychophysical range of discrimination thresholds. However, they did not develop the sinusoidal trend in perceptual thresholds observed across test motion patterns. If, as we have hypothesized, the trend in threshold performance were due to a combination of neural properties (such as the distribution of preferred motion patterns) inherent to the cells underlying the perceptual task, then we would not have expected the uniform models to deviate significantly from the flat trend obtained across all simulated conditions.

Taken together these results indicate that an independent-response population code is capable of extracting perceptual information relevant to the motion pattern task. However, the model's strong dependence on population size and the distribution of preferred motions prevent this scheme from producing a robust quantitative measure that is consistent with the psychophysical performance reported across observers.

4.2.   Influence of the Preferred Motion-Pattern Distribution on Threshold Discrimination

Across the range of conditions simulated in the model, a clear relationship emerged between the distribution of preferred motion patterns and the resulting trend in discrimination thresholds. Due in part to the near-equal weighting of neural responses in the population vector representation, the trend in discrimination thresholds for independent-response populations was closely matched to the distribution of preferred motion patterns. To a first approximation, this relationship can be explained simply by the proportional increase in the population SNR as a function of the preferred motion pattern density of units responsive to a given test motion.

The introduction of lateral connections that inhibited antipreferred motions modified the resultant trend in thresholds to reflect the relative changes in the population SNR associated with the antipreferred inhibition of neural subpopulations not responding to the stimulus. In this way, anisotropies biased toward expanding patterns of motion maximized contracting pattern discrimination for laterally connected populations by inhibiting the baseline noise contributed to the population vector by the population majority (expansion preferred units). Analogously, when the physiologically reported anisotropy was removed (uniform models), discrimination thresholds remained flat and did not develop statistically significant variations across test motions.

Taken in the context of the preferred motion properties reported in MST, the ability of interconnected neural populations, containing anisotropic preferred motion distributions, to encode the motion information necessary to accurately discriminate small motion differences suggests similar structures may be present in the human visual motion pathway. Furthermore, if the degree of variation in thresholds across test motions is simply an artifact of the underlying neural properties, as proposed here, then a more direct comparison between the perceptual trends and those obtained from the unimodal/bimodal models suggests the presence of an anisotropy whose bias is more closely approximated by the distribution reported in Geesaman and Andersen (1996).

4.3.   Influence of Lateral Connections on Threshold Discrimination

The addition of lateral connections that minimized neural noise within the physiologically simulated

preferred motion-pattern distributions (unimodal and bimodal) produced discrimination thresholds that were well matched with human perceptual performance across test motions. Neural structures containing excitatory and inhibitory lateral connections were able to accurately simulate psychophysical thresholds for populations spanning a 20-fold increase in size (100 to 2,000 units). Equivalent levels of performance were also obtained using larger neural populations that contained *only* inhibitory lateral connections centered on antipreferred neural populations.

Together with the robust encoding of discrimination thresholds reported as a function of the spread of excitatory connections (σ_E), these results suggest that the sinusoidal trend in psychophysical performance may be mediated primarily through signal enhancement associated with the strength (S_A) and spread (σ_I) of inhibitory connections within an anisotropic distribution of preferred motion patterns. The ability of preferred stimulus units to inhibit nonpreferred units greatly reduced the level of noise across the population, thereby increasing discriminability. This helped offset the strong bias for expanding motion patterns reported in the physiology and produced the cyclic trend in which radial discrimination thresholds were lowest.

Further support for an inhibitory architecture can be found in the performance of the threshold models. As with the various interconnecting architectures proposed here, the thresholded populations were able to accurately approximate human performance for moderately large neural populations (>500 units).

Although this strategy for reducing noise is computationally appealing, the simulations suggest that to be effective it would require a relatively high threshold ($T_R \approx 35$ spikes/s). At this level, much of the visual motion information encoded across the population would be sacrificed to extract the perceptually relevant information. Such an effect cannot be easily reconciled with the correlations reported between perceptual performance and single-cell firing rates in visual motion areas such as MT and MST (Britten et al., 1992; Celebrini and Newsome, 1994). Together with the necessity of *a priori* knowledge regarding what constitutes noise versus signal implicit in this structure, the use of such a mechanism in the perceptual task presented here seems unlikely.

However, the sparse neural representation within these threshold populations does provide some computational insight in that it is similar to a winner-take-all strategy for encoding motion patterns. In

biologically plausible neural structures, such strategies are often implemented using mutually inhibiting lateral connections that suppress all but the strongest neural responses. Taken in the less extreme case of a winner-take-all strategy across neural subpopulations (such as contraction preferred units), the resultant inhibitory structures would be qualitatively similar to the mutually inhibiting connection profiles explicitly simulated here in the laterally connected series of models.

4.4.   *Inhibitory Influences in MST*

Anecdotal physiological support for inhibitory structures within MST that are consistent with those proposed in the model can be found in the literature. Several studies have reported inhibitory effects in the motion-pattern properties of MST neurons, although the degree and specificity of inhibition has not been characterized in detail (Duffy and Wurtz, 1991a; Lappe et al., 1996). Here we have proposed an architecture of local interactions within MST whose visual motion properties are consistent with the available physiological evidence. The model predicts an 80 to 100 deg spread of inhibition (σ_I), as defined in the 2D stimulus space, whose profile is continuous across preferred motion patterns.

Multicellular studies in MST would be well suited to examine this result and further quantify the extent of inhibitory influence across motion-pattern sensitive cells. By correlating neural responses across cell pairs as a function of the relative distances between preferred motion patterns and the retinotopic positions of their receptive field centers, multicellular studies could be used to quantify (1) the spread of inhibition as a function of preferred motion patterns, (2) the extent to which lateral interactions span a continuous profile of relative strength, and (3) the retinotopic extent of lateral interactions.

It is worth noting that while the performance of the laterally connected models suggests the presence of specific interconnecting inhibitory structures between motion-pattern detectors, the inhibitory effects implied by the model *do not* require the massive degree of interconnections implemented here. Equivalent lateral interactions could be achieved in more biologically plausible architectures containing small populations of inhibiting interneurons whose presynaptic inhibition of preferred motion subpopulations follows an anti-Hebbian rule of connection strength. Discrete inhibitory profiles whose strength is constant within

preferred motion subpopulations could also be implemented without seriously degrading the motion-pattern information stored across the population. For equivalent representations of σ_I and/or half-width, in continuous and discrete profiles respectively, the influence of the antipreferred inhibitory structures would likely be similar such that discrimination thresholds continued to be well matched to human perceptual performance.

4.5. Neural Interactions Within and Across Visual Motion Areas

The gross increase in computational complexity observed along the visual motion pathway has typically been associated with a feed-forward pooling of visual motion information *between* visual areas. In this scheme, neural responses to simple visual motion components are combined to encode more complex and perceptually relevant properties of the visual scene.

The model presented here does not explicitly preclude the existence of inhibitory feed-forward structures in the projection of motion information from MT to MST. While it is possible to obtain similar computational results using feed-forward mechanisms that inhibit global motion pattern responses via convergent local motion inputs, the mechanisms underlying the development of such a system remain unclear. In a previous neural model of motion-pattern processing (Beardsley and Vaina, 1998) we illustrated the development of lateral inhibition between MST-like units under a supervised learning rule. We also reported anecdotal evidence of inhibitory local motion projections whose development appeared to be linked to the underlying learning rule. It seems likely that the visual motion pathway contains a combination of both inhibitory feed-forward and lateral connections between cells that act to maintain the visual information encoded across noisy neural populations. Future extensions of this model to include a feed-forward layer of direction selective MT inputs and physiological studies by others incorporating multicellular recording techniques within and across visual motion areas could be well suited to address these questions in greater detail.

4.6. Relation to Existing Models of MST

As we alluded to in the introduction, numerous feed-forward models of MT-MST visual motion pooling have been developed whose unit responses are consistent with cells in MST and can be used to extract perceptually relevant visual motion estimates. Three in particular, Perrone and Stone (1994, 1998), Zemel and Sejnowski (1998), and Lappe et al. (1996), contain many of the underlying visual motion properties assumed here and could, in principle, also be used to model GMP threshold performance. In practice, the methods employed in each model may in some ways restrict their extension to graded pattern discriminations, but in doing so they are likely to provide useful insights into the computational and structural requirements of higher-dimensional encoding and perceptual decoding across multiple visual motion tasks.

In the template model of heading estimation forwarded by Perrone and Stone (1994, 1998), perceptual estimates are obtained according to the gaze-stabilized translation properties of the most active template unit. In this case much of the visual motion information encoded across the population is discarded, removing a potential source of correlated signal that could be used to compensate the effects of internal and/or external noise. While such methods also have the advantage of removing much of the population noise, the tradeoff in perceptual performance is strongly dependent on the underlying computational structure and physiological properties. As a result it is unclear how perceptual performance would degrade as a function of neural and visual motion noise. Specifically, can maximal unit responses accurately decode the percept under noisy conditions, or is it necessary to make more explicit use of the visual signal encoded across the population as a whole?

Other models, including Zemel and Sejnowski (1998), Lappe et al. (1996), Lappe and Duffy (1999), and Lappe and Rauschecker (1993, 1995), have decoded perceptual estimates based on the maximal activity obtained across neural subpopulations. While the signal integration afforded such methods is likely to provide a computationally more robust perceptual estimate under noisy conditions, in the case of GMP discrimination it is not immediately clear how many neural subpopulations might be required nor how many units each should contain.

Together with the extension of the population model presented here, to include a feed-forward layer of MT projections, these models could be readily extended to examine GMP discrimination across a wide range of stimulus conditions. In doing so each would provide additional insight into the relative roles of feed-forward versus lateral connections and the range of

decoding schemes necessary to decode equivalent measures of human perceptual performance. Specifically, to what extent might inhibitory feed-forward projections be used to mediate the decoded motion patterns? And what limitations do existing decoding strategies place on the extraction of perceptually equivalent measures of human performance in the presence of noise (internal and external) and across multidimensional parameter spaces associated with multiple perceptual tasks?

Within the visual cortex, the use of experimental and computational techniques to investigate neural connectivity continues to refine the role of intrinsic lateral connections in the emergent computational and perceptual properties of the visual system. The model we have presented here builds on and extends these concepts to cortical areas later in the visual motion pathway. Through simulated populations of MST-like units we have identified a set of antipreferred inhibitory structures whose computational effects on the encoded motion pattern information are well matched to equivalent measures of perceptual performance. These structures are qualitatively similar to the inhibition of antipreferred direction tuned cells reported in earlier visual motion areas such as MT and suggest a more a complex neural architecture throughout the visual motion system.

Acknowledgments

Note

1. Centroid coordinates along the independent parameter axes (σ_I and S_A) were estimated using a center-of-mass calculation within the correlation map's ROI ($r > 0.8r_{max}$). For correlations (R) across independent parameters (x, y) the general calculation of the centroid is $X_C = \Sigma(X R_{x,y})/\Sigma(Rx, y)$ and $Y_C = \Sigma(Y R_{x,y})/\Sigma(R_{x,y})$, respectively.

References

Adini Y, Sagi D, Tsodyks M (1997) Excitatory-inhibitory network in the visual cortex: Psychophysical evidence. *Proc. Natl. Acad. Sci.* 94:10426–10431.

Amir Y, Harel M, Malach R (1993) Cortical hierarchy reflected in the organization of intrinsic connections in macaque monkey visual cortex. *J. Comp. Neurol.* 334:19–46.

Andersen RA (1997) Neural mechanisms of visual motion perception in primates. *Neuron* 18:865–872.

Andersen RA, Shenoy KV, Crowell JA, Bradley DC (2000). Neural mechanisms for self-motion perception in area MST. In: *Neuronal Processing of Optic Flow*. Academic Press, New York, pp. 219–234.

Beardsley S, Clifford C, Vaina LM (1999) Discrimination of complex motion patterns is consistent with an interconnected population code in MST [ARVO Abstract]. *Invest. Ophthalmol. Vis. Sci.* 40:S4222. Abstract 2226.

Beardsley S, Vaina L (1998) Computational modeling of optic flow selectivity in MSTd neurons. *Network: Comput. Neural Syst.* 9:467–493.

Beardsley S, Vaina LM (2001) Discriminating complex pattern motions: Psychophysical evidence for a global motion mechanism. In preparation.

Ben-Yishai B, Bar-Or RL, Sompolinsky H (1995) Theory of orientation tuning in visual cortex. *Proc. Natl. Acad. Sci.* 92:3844–3848.

Bremmer F, Duhamel J-R, Ben Hamed S, Werner G (2000) Stages of self-motion processing in primate posterior parietal cortex. In: *Neuronal Processing of Optic Flow*. Academic Press, New York, pp. 173–198.

Britten KH, Shadlen MN, Newsome WT, Movshon JA (1992) The analysis of visual motion: A comparison of neuronal and psychophysical performance. *J. Neurosci.* 12:4745–4765.

Burr DC, Morrone MC, Vaina LM (1998) Large receptive fields for optic flow detection in humans. *Vision Res.* 38:1731–1743.

Cameron S, Grossberg S, Guenther FH (1998) A self-organizing neural network architecture for navigation using optic flow. *Neural Comput.* 10:313–352.

Celebrini S, Newsome W (1994) Neuronal and psychophysical sensitivity to motion signals in extrastriate area MST of the macaque monkey. *J. Neurosci.* 14:4109–4124.

Chey J, Grossberg S, Mingolla E (1998) Neural dynamics of motion processing and speed discrimination. *Vision Res.* 38:2769–2786.

deCharms RC, Zador A (2000) Neural representation and the cortical code. *Ann. Rev. Neurosci.* 23:613–647.

Duffy CJ (2000) Optic flow analysis for self-movement perception. In: *Neuronal Processing of Optic Flow*. Academic Press, New York, pp. 199–218.

Duffy CJ, Wurtz RH (1991a) Sensitivity of MST neurons to optic flow stimuli. I. A continuum of response selectivity to large-field stimuli. *J. Neurophysiol.* 65:1329–1345.

Duffy CJ, Wurtz RH (1991b) Sensitivity of MST neurons to optic flow stimuli. II. Mechanisms of response selectivity revealed by small field stimuli. *J. Neurophysiol.* 65:1346–1359.

Duffy CJ, Wurtz RH (1995) Response of monkey MST neurons to optic flow stimuli with shifted centers of motion. *J. Neurosci.* 15:5192–5208.

Duffy CJ, Wurtz RH (1997) Planar directional contributions to optic flow responses in MST neurons. *J. Neurophysiol.* 77:782–796.

Edelman S (1996) Why have lateral connections in the visual cortex? Lateral interactions in the cortex: Structure and function. The UTCS Neural Networks Research Group. Austin. http://www.cs.utexas.edu/users/nn/web-pubs/htmlbook96/edelman/.

Foldiak P (1993) The 'ideal homunculus'. Statistical inference from neural population responses. In: *Computation and Neural Systems.*

Kluwer Academic Publishers, Norwell, pp. 55–60.

Freeman TC, Harris MG (1992) Human sensitivity to expanding and rotating motion: Effects of complementary masking and directional structure. *Vision Res*. 32:81–87.

Geesaman BJ, Andersen RA (1996) The analysis of complex motion patterns by form/cue invariant MSTd neurons. *J. Neurosci*. 16:4716–4732.

Georgopoulos AP, Kettner RE, Schwartz AB (1988) Primate motor cortex and free arm movements to visual targets in three-dimensional space. II. Coding of the direction of movement by a neuronal population. *J. Neurosci*. 8:2928–2937.

Georgopoulos AP, Schwartz AB, Kettner RE (1986) Neuronal population coding of movement direction. *Science* 233:1416–1419.

Gilbert C (1992) Horizontal integration and cortical dynamics. *Neuron* 9:1–13.

Gilbert C, Das A, Ito M, Kapadia M, Westheimer G (1996) Spatial integration and cortical dynamics. *Proc. Natl. Acad. Sci. USA* 93:615–622.

Graziano MS, Anderson RA, Snowden R (1994) Tuning of MST neurons to spiral motions. *J. Neurosci*. 14:54–67.

Grossberg S, Mignolla E, Pack C (1999) A neural model of motion processing and visual navigation by cortical area MST. *Cerebral Cortex* 9:1–18.

Hatsopoulos N, Warren WJ (1991) Visual navigation with a neural network. *Neural Networks* 4:303–317.

Haykin S (1999) *Neural Networks: A Comprehensive Foundation*. Prentice Hall, Upper Saddle River, NJ.

Hertz J, Krogh A, Palmer RG (1991) *Introduction to the Theory of Neural Computation*. Addison-Wesley, New York.

Kalaska JF, Caminiti R, Georgopoulos AP (1983) Cortical mechanisms related to the direction of two-dimensional arm movements: Relations in parietal area 5 and comparison with motor cortex. *Exp. Brain Res*. 51:247–260.

Kisvarday Z, Toth E, Rausch M, Eysel U (1997) Orientation-specific relationship between populations of excitatory and inhibitory lateral connections in the visual cortex of the cat. *Cereb. Cortex* 7:605–618.

Koechlin E, Anton J, Burnod Y (1999) Bayesian interference in populations of cortical neurons: A model of motion integration and segmentation in area MT. *Biol. Cybern*. 80:25–44.

Lagae L, Maes H, Raiguel S, Xiao DK, Orban GA (1994) Responses of macaque STS neurons to optic flow components: A comparison of areas MT and MST. *J. Neurophysiol*. 71:1597–626.

Lappe M (2000) Computational mechanisms for optic flow analysis in primate cortex. *Neuronal Processing of Optic Flow*. Academic Press, New York, pp. 235–268.

Lappe M, Bremmer F, Pekel M, Thiele A, Hoffmann K (1996) Optic flow processing in monkey STS: A theoretical and experimental approach. *J. Neurosci*. 16:6265–6285.

Lappe M, Bremmer F, van den Berg AV (1999) Perception of self-motion from visual flow. *Trends in Cognitive Sciences* 3:329–336.

Lappe M, Duffy C (1999) Optic flow illusion and single neuron behavior reconciled by a population model. *Eur. J. Neurosci. im Druck*.

Lappe M, Rauschecker JP (1993) A neural network for the processing of optic flow from ego-motion in man and higher mammals. *Neural Comp*. 5:374–391.

Lappe M, Rauschecker JP (1995) An illusory transformation in a model of optic flow processing. *Vision Res*. 35:1619–1631.

Liu L, Hulle V (1998) Modeling the surround of MT cells and their

selectivity for surface orientation in depth specified by motion. *Neural Comput*. 10:295–312.

Lukashin AV, Georgopoulos AP (1993) A dynamical neural network model for motor cortical activity during movement: Population coding of movement trajectories. *Biol. Cybern*. 69:517–524.

Lukashin AV, Georgopoulos AP (1994) A neural network for coding of trajectories by time series of neuronal population vectors. *Neur. Comp*. 6:19–28.

Lukashin AV, Wilcox GL, Georgopoulos AP (1996) Modeling of directional operations in the motor cortex: A noisy network of spiking neurons is trained to generate a neural-vector trajectory. *Neural Networks* 9:397–410.

Lund J, Yoshioka T, Levitt J (1993) Comparison of intrinsic connectivity in different areas of the macaque monkey cerebral cortex. *Cereb. Cortex* 3:148–162.

Malach R, Schirman T, Harel M, Tootell R, Malonek D (1997) Organization of intrinsic connections in owl monkey area MT. *Cereb. Cortex* 7:386–393.

Miikkulainen R, Sirosh J (1996) Introduction: The emerging understanding of lateral interactions in the cortex. Lateral interactions in the cortex: Structure and function. UTCS Neural Networks Research Group, Austin. http://www.cs.utexas.edu/users/nn/web-pubs/htmlbook96/miikkulainen/.

Morrone C, Burr D, Vaina L (1995) Two stages of visual processing for radial and circular motion. *Nature* 376:507–509.

Nowlan SJ, Sejnowski TJ (1995) A selection model for motion processing in area MT of primates. *J. Neurosci*. 15:1195–1214.

Oram MW, Foldiak P, Perrett DI, Sengpiel F (1998) The 'ideal homunculus': Decoding neural population signals. *Trends in Neurosci*. 21:365.

Orban GA, Lagae L, Raiguel S, Xiao D, Maes H (1995) The speed tuning of medial superior temporal (MST) cell responses to optic-flow components. *Perception* 24:269–285.

Orban GA, Lagae L, Verri A, Raiguel S, Xiao D, Maes H, Torre V (1992) First-order analysis of optical flow in monkey brain. *Proc. Nat. Acad. Sci*. 89:2595–2599.

Perrone J, Stone L (1994) A model of self-motion estimation within primate extrastriate visual cortex. *Vision Res*. 34:2917–2938.

Perrone JA, Stone LS (1998) Emulating the visual receptive-field properties of MST neurons with a template model of heading estimation. *J. Neurosci*. 18:5958–5975.

Pouget A, Zhang K, Deneve S, Latham PE (1998) Statistically efficient estimation using population coding. *Neural Comput*. 10:373–401.

Regan D, Beverley KI (1978) Looming detectors in the human visual pathway. *Vision Res*. 18:415–421.

Regan D, Beverley KI (1979) Visually guided locomotion: Psychophysical evidence for a neural mechanism sensitive to flow patterns. *Science* 205:311–313.

Regan D, Beverley KI (1985) Visual responses to vorticity and the neural analysis of optic flow. *J. Opt. Soc. Am*. 2:280–283.

Saito H-A, Yukie M, Tanaka K, Hikosaka K, Fukada Y, Iwai E (1986) Integration of direction signals of image motion in the superior temporal sulcus of the macaque monkey. *J. Neurosci*. 6:145–157.

Sakai K, Miyashita Y (1991) Neural organization for the long-term memory of paired associates. *Nature* 354:152–155.

Salinas E, Abbott L (1994) Vector reconstruction from firing rates. *J. Comput. Neurosci*. 1:89–107.

Salinas E, Abbott L (1995) Transfer of coded information from sensory to motor networks. *J. Neurosci*. 15:6461–6474.

Sanger TD (1996) Probability density estimation for the interpretation of neural population codes. *J. Neurophysiol*. 76:2790–2793.

Schwartz AB, Kettner RE, Georgopoulos AP (1988) Primate motor cortex and free arm movements to visual targets in three-dimensional space. I. Relations between single cell discharge and direction of movement. *J. Neurosci*. 8:2913–2827.

Seung HS, Sompolinsky H (1993) Simple models for reading neuronal population codes. *Neurobiol*. 90:10749–10753.

Shadlen M, Newsome W (1994) Noise, neural codes, and cortical organization. *Curr. Opin. Neurobiol*. 4:569–579.

Shadlen M, Newsome W (1998) The variable discharge of cortical neurons: Implications for connectivity, computation, and information coding. *J. Neurosci*. 18:3870–3896.

Snippe H (1996) Parameter extraction from population codes: A critical assessment. *Neural Comp*. 8:511–530.

Snowden RJ, Milne AB (1996) The effects of adapting to complex motions: Position invariance and tuning to spiral motions. *J. Cog. Neurosci*. 8:412–429.

Softky W (1995) Simple codes versus efficient codes. *Curr. Opin. Neurobiol*. 5:239–247.

Softky W, Koch C (1993) The highly irregular firing of cortical cells is inconsistent with temporal integration of random EPSPs. *J. Neurosci*. 13:334–350.

Stemmler M, Usher M, Niebur E (1995) Lateral interactions in primary visual cortex: A model bridging physiology and psychophysics. *Science* 269:1877–1880.

Sundareswaran V, Vaina LM (1995) Perceptual learning of direction discrimination in global motion: Psychophysics and computational modeling [ARVO Abstract]. *Invest. Ophthalmol. Vis. Sci*. 36:S377. Abstract 1782.

Sundareswaran V, Vaina LM (1996) Adaptive computational models of fast learning of motion direction discrimination. *Biol. Cybern*. 74:319–329.

Tanaka K, Fukada Y, Saito H-A (1989) Underlying mechanisms of the response specificity of expansion/contraction and rotation cells in the dorsal part of the medial superior temporal area of the macaque monkey. *J. Neurophysiol*. 62:642–656.

Tanaka K, Saito H (1989) Analysis of motion of the visual field by direction, expansion/contraction, and rotation cells clustered in the dorsal part of the medial superior temporal area of the macaque monkey. *J. Neurophysiol*. 62:626–641.

Taylor JG, Alavi F (1996) A basis for long-range inhibition across cortex. Lateral interactions in the Cortex: Structure and function. UTCS Neural Networks Research Group, Austin. http://www.cs.utexas.edu/users/nn/web-pubs/htmlbook96/taylor/.

Te Pas SF, Kappers AM, Koenderink JJ (1996) Detection of first-order structure in optic flow fields. *Vision Res*. 36:259–270.

Vaina L (1998) Complex motion perception and its deficits. *Curr. Opin. Neurobiol*. 8:494–502.

Vaina L, Sundareswaran V, Harris J (1995) Learning to ignore: Psychophysics and computational modeling of fast learning of direction in noisy motion stimuli. *Cog. Brain Res*. 2:155–163.

van den Berg AV (2000) Human ego-motion perception. In: *Neuronal Processing of Optic Flow*. Academic Press, New York, pp. 3–25.

Wang R (1995) A simple competetive account of some response properties of visual neurons in area MSTd. *Neural Comp*. 7:290–306.

Wang R (1996) A network model for the optic flow computation of the MST neurons. *Neural Networks* 9:411–426.

Wiskott L, von der Malsburg C (1996) Face recognition by dynamic link matching. Lateral interactions in the cortex: Structure and function. UTCS Neural Networks Research Group, Austin. http://www.cs.utexas.edu/users/nn/web-pubs/htmlbook96/wiskott/.

Worgotter F, Niebur E, Christof K (1991) Isotropic connections generate functional asymmetrical behavior in visual cortical cells. *J. Neurophys* 66:444–459.

Zemel R, Dayan P, Pouget A (1998) Probabilistic interpretation of population codes. *Neural Comp*. 10:403–430.

Zemel RS, Sejnowski TJ (1998) A model for encoding multiple object motions and self-motion in area MST of primate visual cortex. *J. Neurosci*. 18:531–547.

Zhang K, Sereno M, Sereno M (1993) Emergence of position-independent detectors of sense of rotation and dilation with Hebbian learning: An analysis. *Neural Comp*. 5:597–612.

Zohary E (1992) Population coding of visual stimuli cortical neurons tuned to more than one dimension. *Biol. Cybern*. 66:265–272.